AD-760 017

RELATION BETWEEN PARTICULATE CHEMISTRY AND CERAMIC PROPERTIES

Avco Corporation

Prepared for:

Office of Naval Research

March 1973

RELATION BETWEEN PARTICULATE CHEMISTRY AND CERAMIC PROPERTIES

FINAL TECHNICAL REPORT

1 January 1970 - 31 December 1972

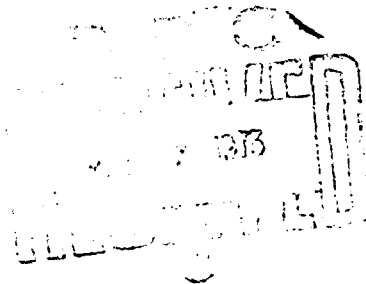Contract N00014-70-C-0138

Prepared by

W.H. Rhodes
B.J. Wuensch
T. Vasilos

Prepared for

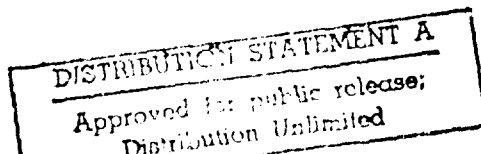Office of Naval Research
Washington, D.C. 20360

Submitted by

AVCO CORPORATION
Systems Division
Lowell, Massachusetts 01851

NATIONAL TECHNICAL
INFORMATION SERVICE

DOCUMENT CONTROL DATA · R & D

(Security classification of title, body of abstract and indexing annotation must be entered when the overall report is classified)

1. ORIGINATING ACTIVITY (Corporate author)	2a. REPORT SECURITY CLASSIFICATION
Avco Corporation Systems Division Lowell, Massachusetts 01851	Unclassified
	2b. GROUP

3. REPORT TITLE

Relation Between Particulate Chemistry and Ceramic Properties

4. DESCRIPTIVE NOTES (Type of report and inclusive dates)

Final Technical Report, 1 January 1970 - 31 December 1972

5. AUTHOR(S) (First name, middle initial, last name)

Rhodes, William H.
Wuensch, Bernhardt J.
Vasilos, Thomas

6. REPORT DATE	7a. TOTAL NO. OF PAGES	7b. NO. OF REFS
March 31, 1973	49 /106	24
8a. CONTRACT OR GRANT NO. N00014-70-C-0138	9a. ORIGINATOR'S REPORT NUMBER(S)	
b. PROJECT NO.		
c.	9b. OTHER REPORT NO(S) (Any other numbers that may be assigned this report)	
d.		

10. DISTRIBUTION STATEMENT

Reproduction in whole or in part is permitted for any purpose of the U.S. Government. Distribution of this document is unlimited.

11. SUPPLEMENTARY NOTES	12. SPONSORING MILITARY ACTIVITY
	Department of the Navy Office of Naval Research Washington, D.C. 20360

13. ABSTRACT

In a program designed to inter-relate the chemistry and morphology of initial particulates with microstructure development and mechanical properties of the final product, it was found that the powder precursor may have an important influence on microstructure. Vacuum hot pressed high purity MgO derived from $Mg(OH)_2$ displayed a marked duplex microstructure and a mean grain size thirty times larger than that in bodies fabricated from carbonate-derived material of the same purity and initial particle size. The duplex structure evolved early in the course of consolidation (less than 70% density) and is attributed to the high degree of mutual orientation of MgO crystallites within relics of the parent brucite plate. Equiaxed, dense microstructures of $Mg_{0.995}Ca_{0.005}O$ were prepared by calcination of coprecipitated carbonates and display grain size smaller than the high purity material under comparable processing cycles. Evidence of a partially-penetrating grain boundary phase was found. Grain growth rates at 1520 and 1310°C decrease rapidly with time due to transition from boundary-controlled to pore-controlled to abnormal grain growth. Room temperature measurements of delayed fracture in three different environments were determined for high purity vacuum hot pressed MgO derived from the carbonate, and compared with results for less pure materials. The high purity magnesia displayed higher resistance to stress corrosion and a higher static fatigue limit than any other grade of material examined.

DD FORM 1473 REPLACES DD FORM 1473, 1 JAN 64, WHICH IS OBSOLETE FOR ARMY USE.

UNCLASSIFIED

Security Classification

Best Available Copy

FOREWORD

This report was prepared by the Systems Division of Avco Corporation under Contract N00014-70-C-0138 with the U.S. Office of Naval Research. The work was administered under the direction of Dr. Arthur Diness, Office of Naval Research.

The report summarizes work conducted from 1 January 1970 to 31 December 1972. Two publications will result from the investigation: "A Relation Between Precursor and Microstructure in MgO" (which will be submitted to the Journal of the American Ceramic Society) and "Stress-Corrosion Cracking in Polycrystalline MgO" (which will be presented at the symposium, "Fracture Mechanics of Ceramics," University Park, Pa., July 1973, and published in the Proceedings of that conference). Manuscripts to be submitted for these two publications are attached as Appendices A and B, respectively. The results contained therein are only briefly summarized in the body of this report.

The authors are pleased to acknowledge the contributions of a number of workers at Avco Systems Division to the program: J. Centorino and J. Zgrebnak for materials preparation, R. Gardner and P. Fuce for ceramographic preparation, C.L. Houck for electron microscopy and P. Berneburg for x-ray studies.

TABLE OF CONTENTS

LIST OF ILLUSTRATIONS

LIST OF TABLES

I. INTRODUCTION

Polycrystalline bodies are involved in nearly all applications of ceramics. The technologically-important properties of these materials are, in large part, determined by their microstructure. The relation between mechanical properties and grain size, for example, has long been known. The final microstructure obtained in a body, however, is in turn, dependent upon a number of kinetic processes which occur during fabrication: Grain growth and changes in pore size, distribution and morphology. Grain boundaries are involved in all of these processes. Despite the importance of boundary properties, much remains to be learned about the kinetics of grain boundary migration in ceramics, and the interaction of boundaries with pores and impurities. It has been only recently appreciated, for example, that the impurities normally present in ceramics are commonly segregated at grain boundaries even when present in bulk concentrations as low as 30 ppm.[1] Impurity segregation may give rise to enhanced mass transport at grain boundaries[2] and thus completely modify the kinetics of processes such as creep, oxidation, sintering and electrical conduction. Segregation is similarly known to directly affect properties such as strength and mechanical behavior.[3]

Impurity segregation may thus influence the properties of ceramics at two levels. Certain properties are directly influenced by the chemical and physical state of grain boundaries. On a second level, impurity segregation influences microstructure development, and thus, through its effect during processing, may control those properties which are dependent upon microstructure. (An example is the intentional addition of small amounts of impurity to retard grain growth during sintering. This prevents entrapment of pores within grains and has permitted the sintering of oxides to full theoretical density.) Few studies of boundary-sensitive properties in

ceramics have adequately characterized the physical and chemical state of grain boundaries. Little is known of the relation between the chemistry of the initial particulates from which a ceramic body is formed, and the impurity distribution in the final microstructure. This situation further indicates a need for the evaluation of microstructure development and properties of an ultrapure material which is free, is so far as possible, from the influences of impurity segregation and porosity.

II. OBJECTIVES OF THE PRESENT STUDY

The present report summarizes the results of a three-year program designed to examine the inter-relation of mechanical properties, microstructure evolution and impurity precipitate distribution, on the one hand, with the chemistry and characteristics of the initial particulates from which the ceramic body is formed. Magnesium oxide was selected for study for a number of reasons. The material is of considerable importance (e.g., as a refractory, use as transparent armor, and in high temperature infrared applications). The material has the rocksalt structure of the simpler monovalent alkali halides, and thus might be a model oxide to which understanding of simpler ionic materials might be extended. Several measurements of grain growth kinetics have been made for this material[4-6] which are not in complete accord. Studies of delayed fracture have been conducted with MgO (see Appendix B) and recent results[7] indicate that this important property is highly sensitive to purity and the chemical state of grain boundaries. Selection of MgO for study was also attractive since extensive data are available[8] for the rates of diffusion of several of the impurity (e.g., Ca, Al, Fe) cations commonly present in commercial grade magnesia. Such data were considered to be of potential value in the interpretation of the rates of impurity segregation and redistribution.

The specific aims of the program were

1. The preparation and characterization of ultrapure MgO
   particulates and also particulates which had been
   homogeneously doped with controlled amounts of
   impurity.

2. Consolidation of the particulates into fully dense
   bodies which were pore-free and which had both a
   fine and uniform grain size.

3. Examination of microstructure evolution and iso-
   thermal grain growth kinetics for the materials
   which were produced.

4. Correlation of mechanical properties (namely. delayed
   fracture) with specimen purity and microstructure.

The results obtained in the program are discussed in Section III.
The most significant findings are that, in the absence of notable impurity,
the development of microstructure in MgO depends markedly on the physical
arrangement of the particulates from which the body is formed, and hence
on the precursor material. The rate of stress-corrosion cracking in
polycrystalline MgO depends markedly on purity. The high purity material
synthesized in this program exhibited a much higher resistance to delayed
fracture in H_2O and a higher static fatigue limit than any other grade of
material which has been examined. Delayed fracture in the latter materials
is attributed to control by interaction of OH^- with crack tips lying in a
calcium aluminosilicate grain boundary phase. These results are discussed
in detail in manuscripts attached as Appendices A and B.

III. RESULTS

3.1 Powder Preparation and Characterization

-4-

3.1.1 Starting Materials

Consolidation of particulates into a fully dense microstructure requires a highly reactive powder with submicron particle size. Examination of products available from commercial sources failed to reveal a high purity (99.99% MgO) submicron magnesia. High purity brucite, $Mg(OH)_2$. and $MgCO_3$ were, however, available. Production of MgO particles with the desired characteristics was, therefore, attempted through the development of controlled calcination procedures.

$Mg(OH)_2$ and $MgCO_3$ powders* and consolidated products were analyzed by spark source mass spectrometry (Table I). The spark source concentrations were higher than the vendors' emission analysis and indicated the presence of significant anion impurity, notably S. The $Mg(OH)_2$ was further characterized by x-ray diffraction and found to be entirely brucite. Electron microscopy revealed a plate-like morphology for the brucite, Figure 1.

3.1.2 Calcination

The decomposition of $Mg(OH)_2$ and $MgCO_3$ to magnesia was studied in an electron microscope under the influence of heating caused by the electron beam, and also as a function of time and temperature for powders heated in vacuum while both static and while rotated.

Examination of the decomposition of brucite. $Mg(OH)_2$ plates under heating induced by the beam of an electron microscope showed the reaction to be topotactic. Figure 2a presents an initial c-axis electron diffraction pattern of a parent brucite crystal. The strong reflections are 100 and 110 brucite maxima. A few weak MgO maxima are present, but the 220 reflection

---

* Purchased from Johnson-Matthey through United Mineral Cor. (U.S. Distribution).

20,000X

Figure ... Electron Micrograph Showing Platy
Morphology of Initial High Purity
Sodium Ni(OH)$_2$ Powder.

TABLE I

CHEMICAL ANALYSIS OF INITIAL POWDERS AND RESULTING PRODUCT

	Mg(OH)$_2$				MgCO$_3$		
	(Emission Spectrography)		Present Work (Spark Source Mass Spectrometry)		Vendor Analysis (Em. Spec.)	Present Work (Spark Source Mass Spectroscopy)	
Element	Lot SH194*	Lot SH182*	Lot SH182*	Hot Pressed Sample 1330 from Lot SH182	Lot 5.7696	Lot 5.7696	Hot Pressed Sample 1117
Al	1	1	4	4	1	20	20
Ca	1	1	100	100	3	30	30
Cl			10	3	-	5	5
Cr	1	1	5	3	-	10	5
B			130	10	-	70	40
Au	1	1	1	1	1	1	1
Zn			3	20	-	7	3
Fe	10	10	4	20	10	30	100
Pb	30	30	4	0.6	-	0.3	15
Si	1	1	150	150	-	10	15
Mn	5	5	1	1	-	7	4
Na	1	1	1500	40	1	2	2

is notably absent upon further decomposition, Figure 2b. 220 MgO reflections appear on the same radius vectors as 110 brucite. The 220 magnesia reflections became more resolved from 110 brucite as decomposition progressed, and the brucite pattern gradually diminished in overall intensity. Eventually, Figure 3c, a $[111]$ axis single crystal MgO pattern resulted. These observations confirm the results of Gordon and Kingery[9] who reported that periclase formed from brucite through a coherent nucleation and growth process, with $[111]$ and $[110]$ of periclase parallel to c and a of brucite, respectively.

Production of powders for eventual consolidation was accomplished through calcination in partial vacuum. The characteristics of the particulates produced was established as a function of time and temperature over a range of 350 to 1200°C.

Static calcinations were performed with the precursor powders loosely packed in a 2 mm bed. The periclase crystallites were found to be oriented within a relic of the parent brucite plate. Such plates, in turn, were agglomerated in groups over an order of magnitude larger. Figure 3, for example, presents electron micrographs of products produced at 375°C. Calcination for 55 minutes produced 10 micron agglomerates composed of multi-crystal relics of 0.8 microns. The particle size within the relics was estimated to be of the order of 100 Å through x-ray line-broadening measurements. This general size was confirmed through direct examination of the relics in high magnification micrographs. Extension of the calcination to 180 minutes produced rod-like crystallites, Figure 3b. A few small MgO particles have fractured apart from the relic, possibly as a result of strain caused by the decrease in molar volume accompanying the coherent nucleation and growth process. Consolidation of the particulates produced in this fashion resulted in duplex microstructures, as discussed below.

#67661   a   120,000X

#68141   b   60,000X

Figure 3.   Arrangement of MgO Crystallites Within a Relic of
            the Parent Brucite Plate after Static Calcination of
            (a) 375°C for 55 Minutes and (b) 375°C for 180
            Minutes.

This was attributed in part to the agglomeration, and high orientation of crystallites within the brucite relic. Retention of OH^- was also suspected of having a possible influence. Subsequent efforts were, therefore, devoted to dynamic, rotary calcinations in an attempt to break up agglomerates. Further, in an attempt to eliminate the possibility of traces of OH^- in subsequent microstructure development, the range of calcination temperatures was extended to those much higher (to $1200^{\circ}C$) than required to decompose $Mg(OH)_2$.

Rotary calcinations were initially performed within a new platinum cylinder positioned at an incline of 20°. The cylinder, in turn, was held within a closed-end high purity alumina tube which was evacuated and rotated at 4 rpm during calcinations at temperatures up to $1200^{\circ}C$. Eventually, to facilitate production of powders in the volume necessary to prepare large-diameter pressings, a larger capacity continuous apparatus was specially constructed.

Figure 4 illustrates the change in crystallite size and agglomeration produced through rotary calcination of $Mg(OH)_2$ for constant time (1 hour) at gradually increased temperature. At $800^{\circ}C$ (Figure 4a) calcination produced a mean crystallite size of 260 Å. Some agglomerates (arrow, in Figure 4a), while polycrystalline, appear to have sintered into a tight aggregate which is suspected (as a result of subsequent observations of microstructure after consolidation) of serving as a seed for secondary grain growth. Calcination at $1000^{\circ}C$, Figure 4b did not produce disc-like aggregates; some fracturing appears to have taken place. The high degree of crystallite orientation, however, still persists and is noteworthy. At the highest temperature employed, Figure 4c, the mean crystallite size increased to 360 Å, and evolution of the particles to a cubic morphology has progressed further. Again, the highly oriented relation of crystallites with an aggregate persists.

#70604A   a   80,000X

#70610A   b   80,000X
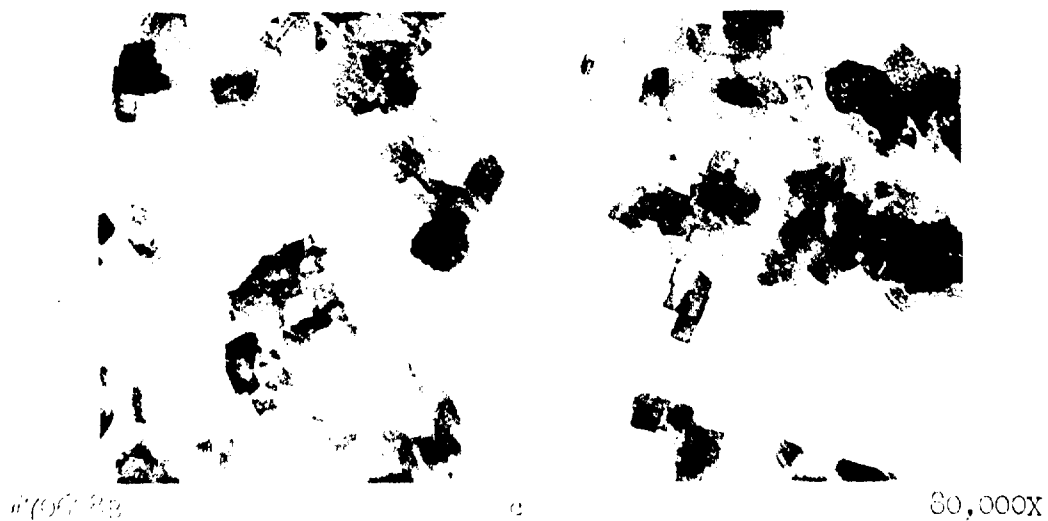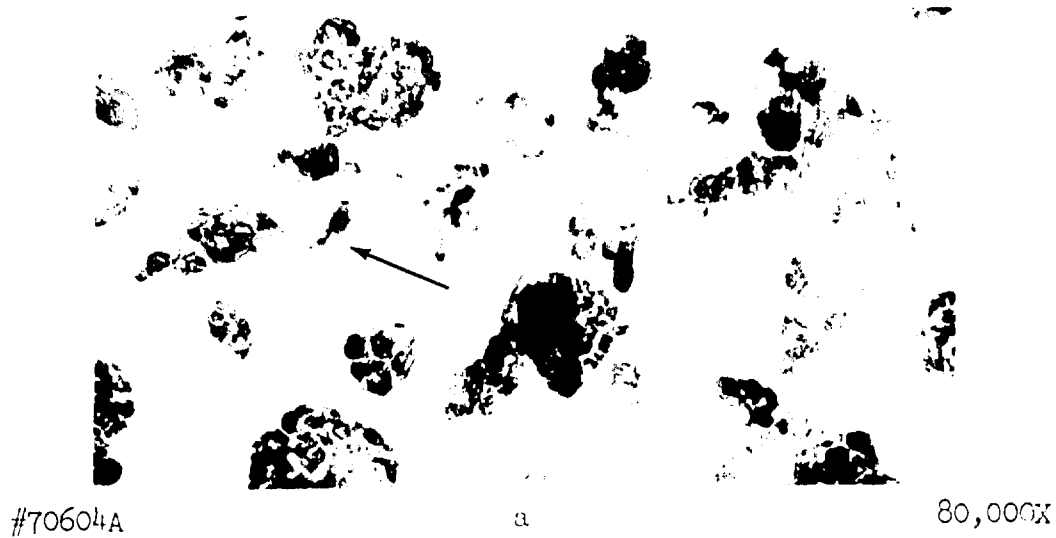
#70612A   c   80,000X

Figure 4. Improvement of MgO Crystallites Produced from Mg(OH)$_2$
Through Rotary Vacuum Calcination for 1 Hour at
(a) ___°C, (b) 1___°C, (c) ___°C.

The distribution of crystallite sizes for the calcination at 120J°C is presented in Figure 5. A plot of the percentage of grains smaller than a given size plotted as a function of particle size yields a linear relation when plotted on log-normal probability paper. The log-normal distribution is to be expected for normal nucleation and growth.

Rotary calcinations were also conducted with reagent grade $MgCO_3$.* Resulting particulates are illustrated in Figure 6 for representative runs conducted at 800°C and 1100°C. The agglomerates produced at 800°C are much larger than those produced with $Mg(OH)_2$ under comparable conditions. The crystallites displayed a cubic morphology, as with $Mg(OH)_2$-derived material at higher temperatures, but the aggregates are much more open. That is, greater space occurs between particles, and the high degree of mutual orientation which is characteristic of the brucite-derived material is not present (see also Figure 1c in Appendix A). Figure 6c contrasts the products of the present study with a MgO powder purchased from Honeywell. This material had been produced by calcination of another reagent-grade $MgCO_3$.** The Honeywell material displaced a larger crystallite size than any product prepared in the present study. Other characteristics, namely the cubic morphology and the random mutual arrangement of crystallites, are similar to those of the present work. The agglomerates in the Honeywell material, however, appear to be somewhat smaller.

Table 2 summarizes the mean crystallite size for several of the calcination treatments which were explored in this program. Examination of the rate of mean particle size increase with reciprocal temperature of

---

* Johnson-Matthey.

**Mallinkrodt.
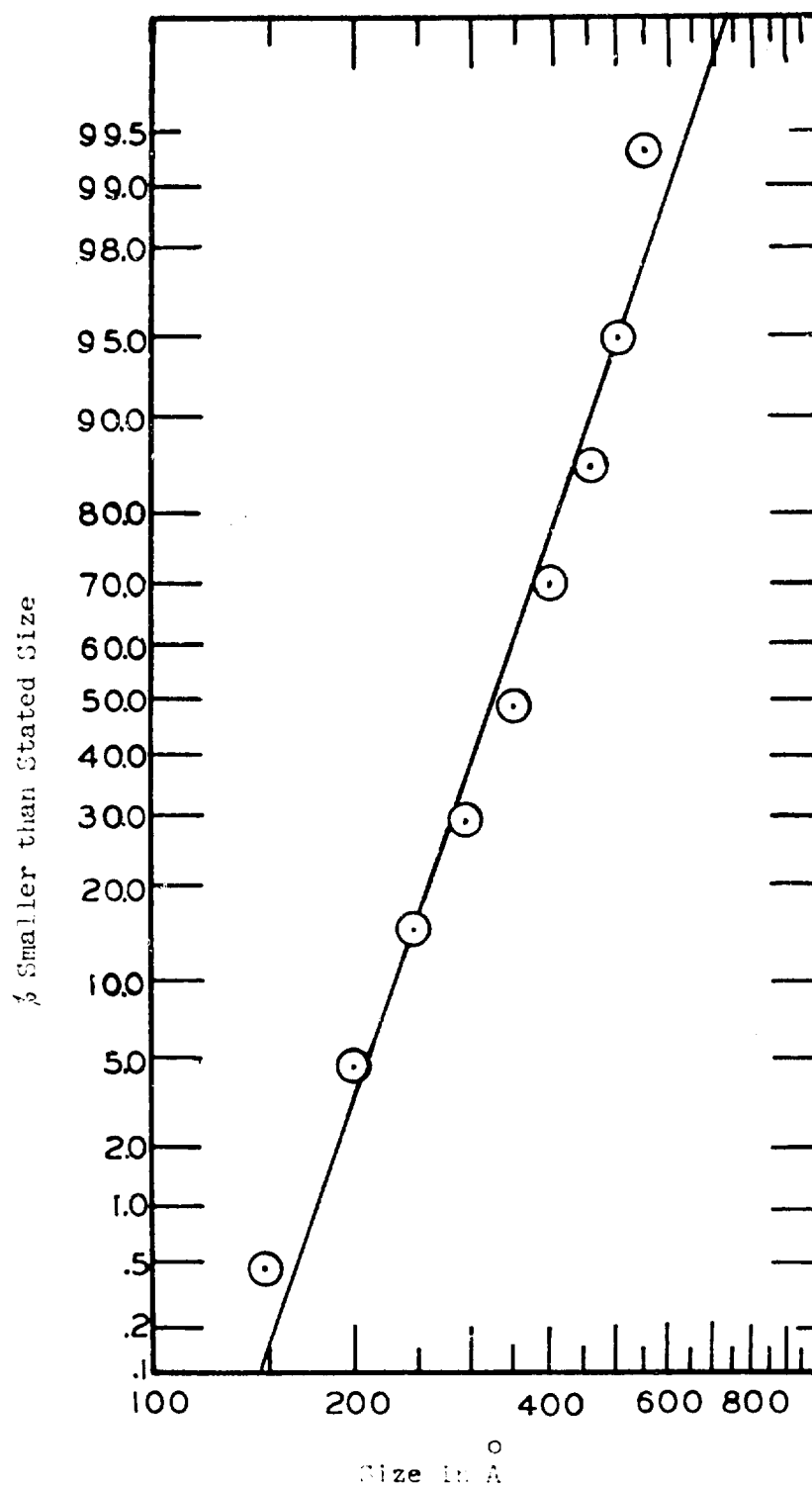
Figure 5. Crystallite Size Distribution for
High-Purity MgO Powder Produced from
$Mg(OH)_2$ Through Rotary Vacuum
Calcination for 1 Hour at $1200^{\circ}C$.

TABLE 2

MgO CRYSTALLITE SIZES PRODUCED UNDER VARIOUS CALCINATION CONDITIONS

Starting Compound	Lot No.	Condition	Temp. °C	Time Min.	Mean Crystallite Size, Å*
Mg(OH)$_2$	SH194**	Static	350	55	ca 100
	SH194	Static	375	55	ca 100
	SH182	Static	375	180	ca 100
	SH194	Static	375	180	ca 100
	SH182	Static	800	60	450
	SH182	Dynamic	800	60	260
	SH182	Dynamic	900	60	263
	SH182	Dynamic	1000	60	278
	SH182	Dynamic	1100	30	288
	SH182	Dynamic	1100	60	293
	SH182	Dynamic	1100	120	299
	SH182	Dynamic	1200	10	333
	SH182	Dynamic	1200	30	358
	SH182	Dynamic	1200	60	363
MgCO$_3$	700752***	Dynamic	800	60	152
	700752	Dynamic	1100	30	318

---

* From x-ray line broadening analysis

** Johnson-Matthey

*** Fisher

calcination indicates an activation energy of only 0.8 eV. This value
is much smaller than the activation energies for cation self-diffusion or
oxygen self-diffusion (2.76^8 and 2.71^{10} eV. respectively). Lattice self-
diffusion thus appears not to be the process controlling particulate growth.

3.1.3 Conversion of Starting Materials

Subsequent experience with consolidation of the particulates,
described in Section 3.2, revealed a marked difference between the micro-
structures produced from $Mg(OH)_2$-derived magnesia and those produced from
the $MgCO_3$ precursor. To determine whether the differing behaviors arose
from minor differences in purity, and thereby clarify the conditions necessary
to obtain high purity, fully dense, fine grained structures, it was decided
to convert one precursor material into the other to permit distribution
between chemical and physical effects.

The ultra-high purity $Mg(OH)_2$ used throughout the calcination
studies was converted to $MgCO_3$ while taking all precautions to maintain
chemical purity. This was accomplished by dissolving $Mg(OH)_2$ in HNO_3
followed by precipitation of the carbonate through addition of NH_4CO_3.
The $MgCO_3$, after rinsing and drying, was calcined at $1100^\circ C$ for 1 hour.
These conditions, as in other runs with the carbonate, provided magnesia
particulates with a mean grain size of aboue 300 $\overset{o}{A}$. This powder was then
consolidated, as discussed below, under conditions identical to those used
in processing a number of those samples which had been produced directly
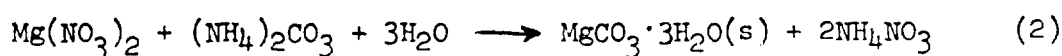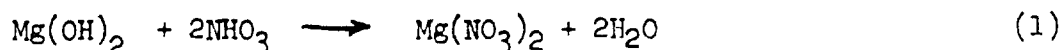from the hydroxide.

3.1.4 Doped Materials

To examine the effects of impurity content upon microstructure
evolution, a set of materials containing controlled additions of typical
impurity were prepared. The traditional ceramic processing techniques of
blending and calcining, or of tumbling, ball milling and pressing were

rejected since this does not produce a dispersion of impurity which is uniform on an atomic scale. Further, these procedures do not usually provide the submicron particle size necessary for consolidation into a uniform, high density structure. The physical requirements for the doped particulates are similar to those demanded of the ultra-high purity materials.

Freeze-drying[11-12] and coprecipitation were selected as principle processes for investigation. An apparatus for the production of freeze-dried precursors was constructed. This process involves spraying of an aqueous solution of soluble salts of the component cations through an aerosol nozzle under the influence of an over-pressure of gas. Argon was employed for the latter purpose. The liquid droplets, homogeneous on an atomic scale, are directed into a chilled bath of an organic liquid with which water is immiscible. The present apparatus employed stirred hexane, in a vacuum flask, maintained at $-76^{\circ}C$ by dry ice-acetone coolant. The liquid droplets freeze rapidly. The solidification process, because of the small size of the drops, occurs rapidly. This prevents exsolution and the solid droplets retain the atomic-scale homogeneity of the initial liquid. After decanting the hexane, the vacuum flask, bearing the still frozen droplets, was connected to a vacuum system equipped with a large liquid N_2 trap for collection of the remaining hexane plus the water of the initial solution. After several hours, the droplets revert to particles of the component salts. and are ready for calcination. Throughout these studies CaO, at a level of 0.5 mole %, was employed as a dopant. Calcium is a common impurity in technical grade MgO. Also, because of its limited solubility in MgO, it is expected to exsolve or segregate at grain boundaries and thus influence microstructure evolution and boundary properties.

The chemistry of several magnesium salt solutions was explored. Attempts initially were directed towards production of a carbonate since, as discussed above, this precursor yielded a desirable product. (All "magnesium" salts had, of course, been combined with the amount of calcium salt necessary to produce the final intended composition $Mg_{0.995}Ca_{.005}O$.) The reactions considered for carbonate formation were

$$Mg(OH)_2 + 2NHO_3 \longrightarrow Mg(NO_3)_2 + 2H_2O \tag{1}$$

$$Mg(NO_3)_2 + (NH_4)_2CO_3 + 3H_2O \longrightarrow MgCO_3 \cdot 3H_2O(s) + 2NH_4NO_3 \tag{2}$$

Precipitation occurs when the addition of $(NH_4)_2CO_3$ brings to solution to the basic side. The initial freeze-drying experiments were conducted with sprayed solutions of a composition close to precipitation under the hope that the carbonate complex would form during reduction of temperature to freezing. Experiments with the nitrate reactions (1) and (2) produced a homogeneously doped freeze-dried magnesium nitrate. This product proved unsatisfactory for the intended purpose since a molten phase resulted during subsequent calcination. The final magnesia produced was large-grained and judged unsuitable for consolidation.

A number of additional starting salts were examined. The chemistries studied are summarized in Table 3. Substitution of chloride salts again resulted in fusion during calcination with an analogous production of large-grained magnesia as a final product. The powder was again judged unsuitable for consolidation and additional experiments were not conducted. Use of sulfates provided more encouraging results, in that a fluffy ammonium magnesium sulfate powder was produced through freeze-drying. Calcination of this product was examined under a range of conditions, Table 4. The

TABLE 3

CHEMISTRIES EMPLOYED IN ATTEMPTS TO FORM UNIFORMLY-DOPED $Mg_{0.995}Ca_{0.005}O$

Technique	Reactants	Freeze-Dried Product	Calcined Product
Freeze-drying	$Mg(NO_3)_2 + (NH_4)_2CO_3$	$Mg(NO_3)_2 \cdot X\ H_2O$	Fused phase developed - unsatisfactory
Freeze-drying	$MgCl_2 + (NH_4)_2CO_3$	$MgCl_2 \cdot X\ H_2O$	Fused phase developed - unsatisfactory
Freeze-drying	$MgSO_4 + (NH_4)_2CO_3$	$(NH_4)_2Mg(SO_4)_2 \cdot 6H_2O$	Calcination to 1300° produced MgO, but minor amounts of $CaSO_4$ and $5MgO \cdot MgSO_4 \cdot 8H_2O$ remained
Freeze-drying	$Mg(C_3H_3O_2)_2 + (NH_4)_2CO_3$	$Mg(C_3H_3O_2)_2 \cdot XH_2O$	MgO - promising
Co-precipitation	$Mg(NO_3)_2 + (NH_4)_2CO_3$	$MgCO_3 \cdot XH_2O$	MgO formed $>1100^\circ C$ - promising. Possibly minor amounts of one unidentified phase

TABLE 4

PRODUCTS PRODUCED BY CALCINATION OF Ca-DOPED FREEZE-DRIED

$(NH_4)_2Mg(SO_4)_2 \cdot 6H_2O$ UNDER VARIOUS CONDITIONS

Calcination Temperature, °C	Phase Analysis	
	Major	Minor
1000	$MgSO_4 \cdot 6H_2O$, $MgSO_4$	MgO
1100	$MgSO_4 \cdot 6H_2O$, $MgSO_4$	MgO
1300	MgO	$CaSO_4$, $5MgO \cdot MgSO_4 \cdot 8H_2O$

sulfate radical appears to be so strongly bonded that calcination above 1300°C seems to be necessary to complete the decomposition. The appearance of a discrete $CaSO_4$ phase at higher temperatures was also disturbing; the higher temperatures apparently permit segregation of the dopant, and thus destroy the initial homogeneity. Furthermore, the magnesia produced by calcination at 1300°C had a mean particle size in excess of 1 micron. This was judged unsuitable for subsequent consolidation. Sulfate reactions were, therefore, dropped from further consideration.

Examination of the literature provides no example of acetates having been used in freeze-drying processes. Such salts were considered to be of interest in that even if the desired $MgCO_3$ product were not produced, magnesium acetate, $Mg(C_3H_3O_2)_2$, itself decomposes to MgO at 320°C. The carbonate complex was found not to form during freeze-drying. The calcium-doped $Mg(C_3H_3O_2)_2 \cdot xH_2O$ produced did, however, calcine nicely to provide a 80 to 90 Å MgO particulate after calcination for only 15 minutes at 600°C. The acetate precursor seems highly satisfactory, and might well be examined in future work directed towards production of doped MgO. Since the carbonate was not formed, future work obviously need not employ the addition of $(NH_4)_2CO_3$. While this approach seems promising, parallel experiments directed towards production of doped $MgCO_3$ through CO-precipitation were conducted as a result of the frustrations encountered in the course of the freeze-dry experiments. Calcium-doped $MgCO_3 \cdot xH_2O$ was successfully prepared through reaction of the nitrates with $(NH_4)_2CO_3$. The product was calcined at 1100°C for 1 hour to yield a doped magnesia with 300 Å crystallite size. This product was eventually produced in volumes sufficient for consolidation through hot pressing. The microstructures produced, and the redistribution of Ca impurity are described in Section 3.2.

## 3.2 Consolidation and Microstructure Evolution

3.2.1 Hot Pressing of Brucite-Derived MgO

Vacuum hot pressing techniques were employed in nearly all consolidation studies of the variety of particulates which were produced. High strength graphite dies* were employed which allowed pressing up to 15,000 psi. The powders were loaded into a 1" diameter die under static-air glove box conditions, placed into the assembly and lightly cold pressed. After evacuation, the sample was heated to 800°C without pressure to allow outgassing. Pressure and temperature were then simultaneously increased until both parameters reached the desired levels. Typical vacuums at peak temperature were of the order of 10^{-4} mm Hg.

Consolidation of the brucite-derived powders were studied under a range of processing conditions which, in extensive prior experience at Avco had succeeded in producing MgO microstructures of near theoretical density, log-normal grain size distributions and mean grain sizes of the order of 9 microns. Pressing temperatures in the range 1150-1450°C. and applied loads up to 15 kpsi were employed. Typical processing cycles ranged in duration from 30 to 120 minutes.

Anomalies were immediately encountered in the densification of the brucite-derived material. Initial specimens employed a lot of high purity powder produced by static calcination at 375°C for 180 minutes. Three microstructures, which are representative of results for the range of temperatures which were employed are compared in Figure 7. A marked duplex microstructure is apparent in Figure 7a. At increased processing temperature, Figure 7b, the concentration of smaller grains decreases; at 1450°C, the highest temperature employed, the fine grains have vanished.
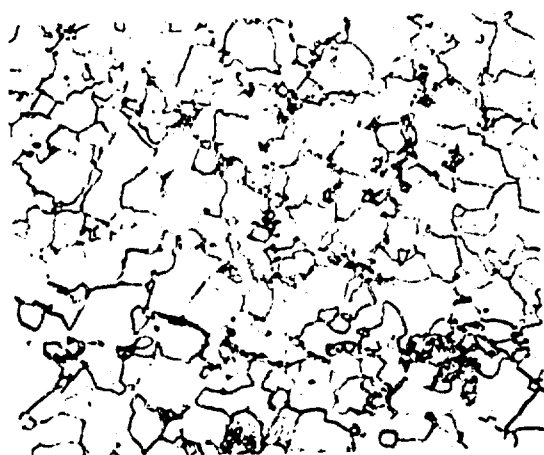
---

* Poco Graphite Co.
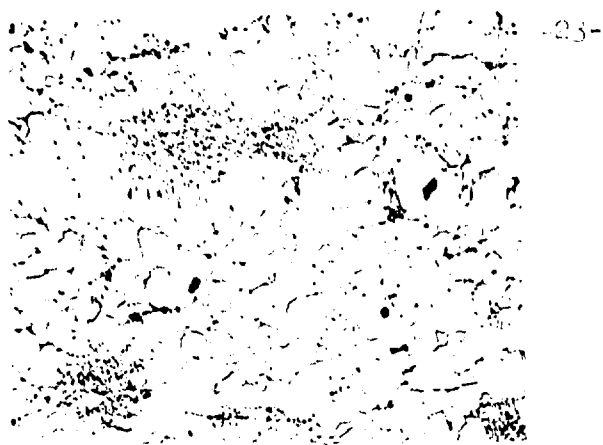
#5014-1   (a)   100X

Hot Pressing Conditions
and Results

SH182 - Mg(OH)$_2$
180 min. static powder calcine
375°C.
1150°C - 15 Kpsi - 90 min.
3.565 gm/cc - 21 μm grain intercept

#5084   (b)   250X

SH182 Mg(OH)$_2$
375°C - 180 min. static powder
calcine
1200°C - 15 Kpsi - 115 min.
3.580 gm/cc - 15 μm grain intercept

(c)   75X

SH194 - Mg(OH)$_2$
375°C - 180 min. static powder
calcine
1450°C - 8 Kpsi - 112 min.
3.583 - 40 μm grain intercept

Figure 7.   Comparison of Microstructures of Three Hot Pressed
Specimens Prepared from Statically Calcined
High Purity Mg(OH)$_2$ Under Different Consolidation
Conditions.

The main variable in producing these distinctly different microstructures was temperature. It is noteworthy that the decrease in the concentrations of fine grains was not accompanied by increase matrix grain-intercept size (21 microns in Figure 7a, 15 microns in Figure 7b). Further, these grain sizes were much larger than those encountered after typical hot pressing cycles using less-pure starting materials. A typical grain size after a 1250°C - 240 minute cycle with 99.4% pure MgO is of the order of 9 microns. The much larger grain sizes of Figure 7 are, at least in part, a consequence of the higher purity.

It was initially felt that the duplex microstructures could be due to patches of incompletely decomposed $Mg(OH)_2$, or, alternatively, related to the state of agglomeration of the magnesia particles within the parent brucite plate. The calcination procedures, as described in Section 3.1.2, were therefore modified to a dynamic process, to break down agglomerates and were extended to temperatures much higher than those required to decompose brucite in an attempt to further reduce concentrations of possible volatiles.

An extensive series of hot pressings were performed with powders produced under the range of dynamic calcining conditions summarized in Table 2. Representative microstructures are compared in Figure 8. The duplex microstructures again invariably resulted. None of the calcining conditions produced a starting powder which gave the desired fine-grained normal microstructures.

It is noteworthy that the chemical integrity of the high purity particulates was maintained during calcination and consolidation. Table 1 compares spark source mass spectrometric analysis of the initial brucite powder and the final consolidation magnesia specimen. It appears that slight
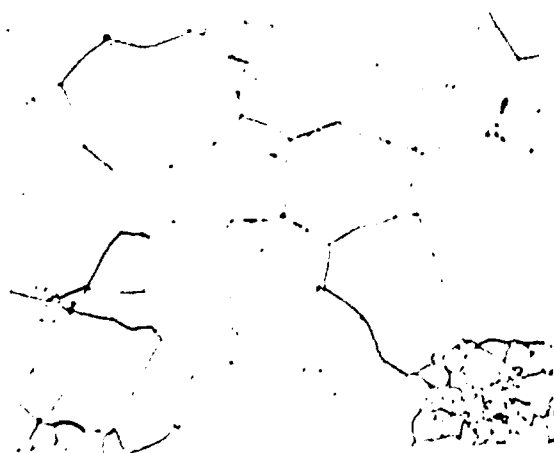
Hot Pressing Conditions
and Results

SH194 Mg(OH)$_2$
800°C - 60 min. static calcine
1150°C - 15 Kpsi - 115 min.
3.569 gm/cc - 10 μm grain intercept

#5351-2   a   750X
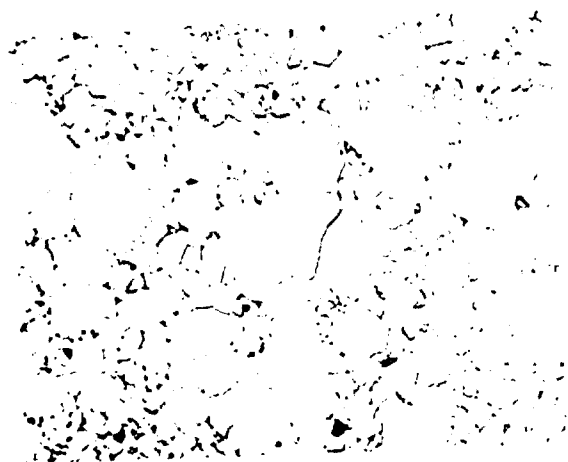
SH182 Mg(OH)$_2$
1200°C - 60 min. dynamic calcine
1155°C - 15 Kpsi - 90 min.
3.586 gm/cc - 6 μm grain intercept

#5351-4   b   750X

SH182 Mg(OH)$_2$
1200°C - 60 min dynamic calcine
1255°C - 15 Kpsi - 30 min.
3.601 gm/cc - 16 μm grain intercept

750X

Figure 8.   Comparison of Microstructures of Hot Pressed MgO
Specimens Prepared from Statically Calcined High
Purity Mg(OH)$_2$, and of Specimens Prepared from
dynamically Calcined Material and Consolidated
Under Various Conditions.

amounts of Zn and Fe are picked up during processing, but that volatiles, notably Cl, S and Na are driven off during consolidation. The total impurity concentration is actually _lower_ in the fabricated sample.

3.2.2 Evolution of Duplex Microstructure

The evolution of the duplex microstructure in the brucite-derived magnesia was studied by deliberately terminating several densification cycles at intermediate levels of density. The microstructures were studied by a combination of light and electron microscopy techniques. Representative micrographs are shown in Figure 9. The sample in Figure 9a was 69% dense. The pores appear to be located primarily at triple-point grain intersections. The grain size, in general, appears to be about 0.3 micron. However, even at this stage there are many grains (e.g., 0.5 micron) which fall outside of the expected normal distribution of grain sizes.

Figure 9b illustrates the microstructure at 92.5% theoretical density. The density is non-uniform. Lens-shaped regions (arrow A) up to 1 mm in size have smaller grain size than the matrix. Other patches (arrow B) have grain sizes about equal to that of the matrix, but a higher porosity which has morphology similar to that at earlier stages of densification. Figure 9c exhibits the microstructure at 99.5% density. The d uplex final structure characteristic of all brucite-derived material has strongly developed. The fine grains have grown to 1 micron, while the large grains are of the order of 30 microns. Some porosity (arrow C) remains associated with the fine grained patches.

The duplex microstructure which appears in brucite-derived material thus evolved during the initial stages of consolidation, at densities less than at most 69% of the theoretical value. It is clear that regions of different density develop during processing. These may contribute to a non-uniform microstructure, but are not believed to be the main cause of this effect.
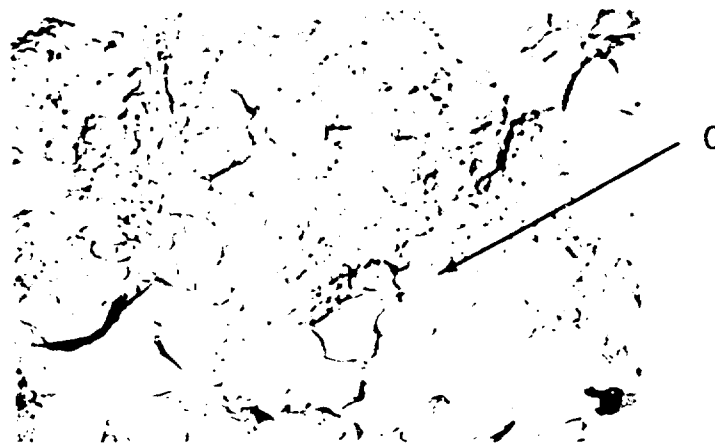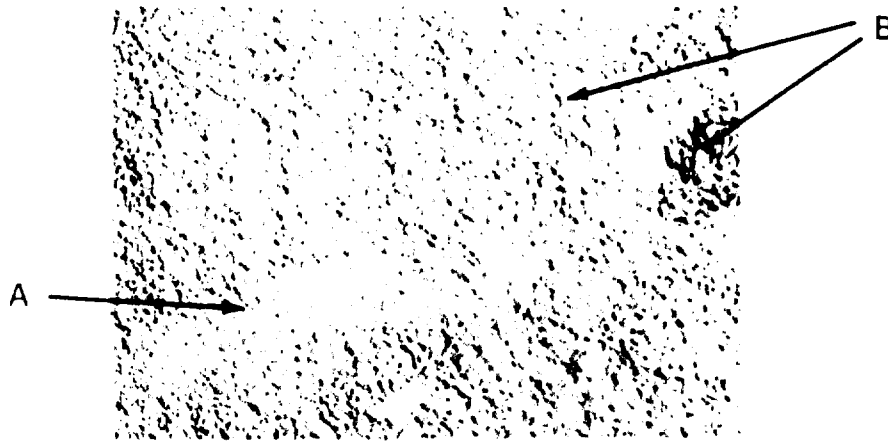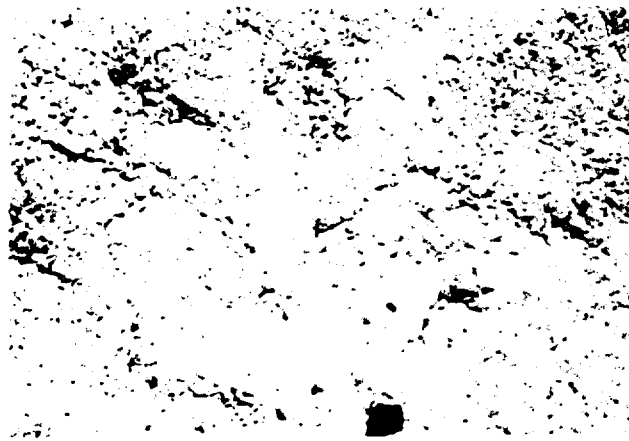
3.2.3 Hot Pressing of MgCO$_3$-Derived MgO

Because of the difficulties encountered in achieving a normal grain structure in Mg(OH)$_2$-derived MgO, studies were conducted on densification of material obtained from MgCO$_3$. The latter compound represented an alternative precursor of ultra-high purity. Consolidation experiments were begun with powders derived from reagent-grade MgCO$_3$. Hot pressing produced fine-grained microstructures with a normal grain size distribution. Since grain growth in these microstructures may have been stabilized by the higher impurity levels, subsequent experiments were conducted with a commercially obtained MgO derived from MgCO$_3$.* Typical analyses of this material, as determined by emission spectroscopy[13] provide approximately 400 ppm impurity, primarily Ca (200), Si (150), Al (50) and Cu (3). The total impurity content is thus similar to that indicated by the mass spectrometric analyses of the hot pressed brucite-derived magnesia. Consolidation studies were eventually performed with powder derived from ultra-high (99.999%) MgCO$_3$**.

All microstructures consolidated from carbonate-derived material were not only similar to one another but differed markedly from the structures obtained from the brucite precursor. Figure 10 compares two microstructures obtained with the Honeywell M-10 powder under different processing conditions. (The sample in Figure 10a displayed a 0.5 micron grain intercept and thus required electron microscopy of an etched microstructure.

The attack of grain boundaries by the etchant unfortunately makes it impossible to examine residual porosity. It is of interest to note that

---

* Honeywell, M-10.

**Johnson-Matthey

Hot Pressing Conditions
and Results

Honeywell - M10
1150°C - 15 Kpsi - 90 min.
3.551 gm/cc - 0.5 μm grain
Intercept
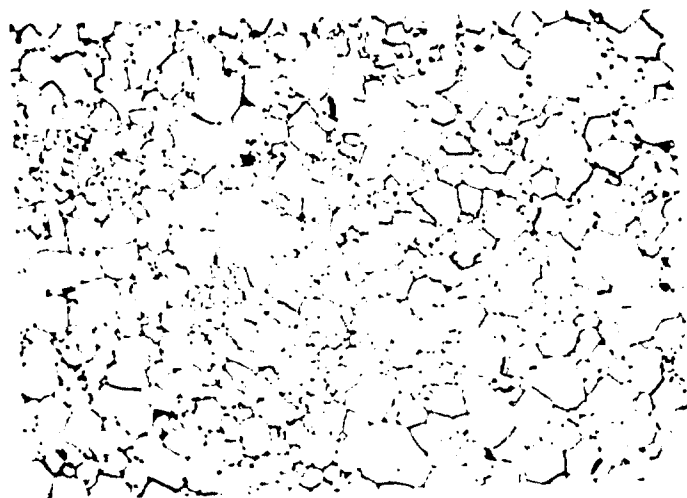
#70693   15.000X

Honeywell - M10
1250°C - 15 Kpsi - 90 min.
3.585 gm/cc - 6 μm grain
Intercept

#5-12-5   50X

Figure 10.   Microstructures of Two MgO Samples Produced from Moderate-
Purity Honeywell M-10 Powder Derived from MgCO₃.

the grain intercept of Figure 10a is smaller, by a factor of more than 30, than the microstructure of Figure 7a, even though both microstructures were consolidated under identical processing cycles. In order to eliminate from consideration the influence of possible absorbed impurities such as OH^- or CO_3^{-2} on microstructure development, the M-10 powder was subjected to a recalcination inasmuch as it had been stored in the calcined condition for over a year. Fifteen grams of the powder were dynamically calcined for 30 minutes at $1000°C$ in vacuum. The product was extracted from the hot furnace, loaded into a die and rapidly placed into the vacuum hot pressing chamber to minimize the possibility of resorption of impurities. Normal grain distributions and grain sizes were obtained upon consolidation of the two powders under similar conditions. The variety of microstructures obtained is thus not dominated by adsorption of impurity by the calcined product. Such adsorption may influence properties[14], but in the present study it does not appear to exert pronounced effects on microstructure development.

3.2.4 Effect of Precursor on Microstructure

The preceding experiments have shown that neither adsorbed impurities, grossly different particle sizes nor differences in purity can account for the difference in final microstructure between samples consolidated from particles derived from $MgCO_3$ and $Mg(OH)_2$. The differences were instead felt to be due to physical rather than chemical differences between the particles derived from the two precursors. As final demonstration of this explanation, and to eliminate the effect of subtle differences in the two precursors, it was decided to convert one precursor into the other, as described in Section 3.1.3. The microstructure produced from the converted carbonate, is compared with a microstructure produced directly from the hydroxide under similar processing conditions in Figure 11. The material produced from the hydroxide again displays the duplex microstructure

SH182 Mg(OH)$_2$ ⟶ MgO
1200°C - 1 hr. dynamic
calcine. 1255°C - 15 Kpsi -
30 min. 3.60 gm/cc -
16 µm grain intercept.

#5412-4   (a)   750X

SH182 Mg(OH)$_2$ ⟶ MgCO$_3$ ⟶ MgO
1100°C - 1 hr. calcine.
1250°C - 15 Kpsi - 90 min.
3.566 gm/cc - 3.4 µm
grain intercept.
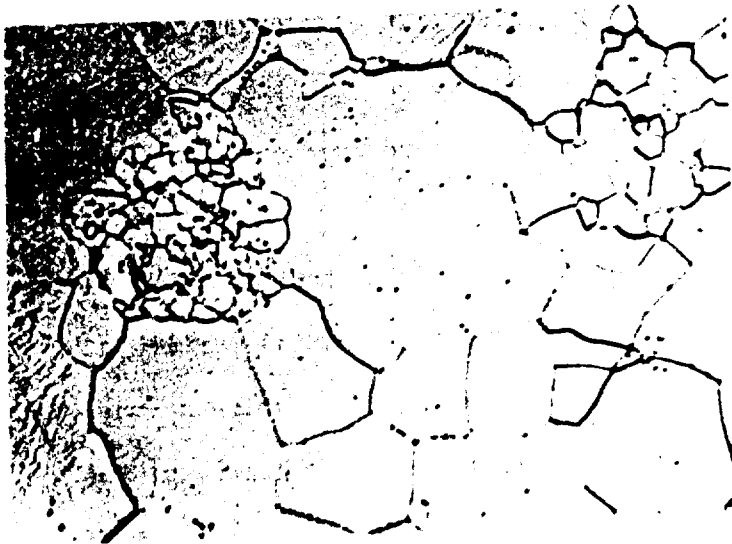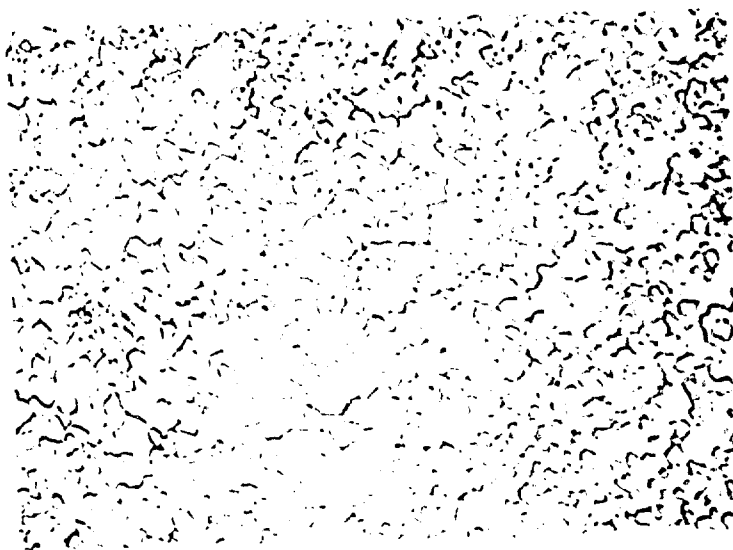
#5525-3   (b)   750X

Figure 11.   Comparison of Microstructures of MgO Prepared from
(a) High Purity Mg(OH)$_2$ and (b) Same Mg(OH)$_2$ Converted
to MgCO$_3$ Before Calcining.

while that produced from the carbonate, as was the case with starting
materials of a range of purity for this precursor, is completely normal.
It is of interest to note that the fine grained patch of Figure 11a has
approximately the same grain size as the normal microstructure of the carbonate-
derived material.

The difference between the hydroxide-and carbonate-derived micro-
structures is attributed to the physical state of the initial particulates
produced by the two precursors. The high degree of mutual orientation
of particles produced from brucite, combined with the high purity of the
material is believed to form a highly-mobile boundary which can rapidly sweep
through an entire agglomerate and thereby form a nucleus for secondary grain
growth. This interpretation is discussed more fully in Appendix A.

3.2.5 Consolidation of Doped Material

As discussed in Section 3.1.4. $MgCO_3$ uniformly doped with 0.
mole % $CaCO_3$ was successfully prepared by a coprecipitation technique.
(A freeze-drying procedure based upon acetates eventually seemed promising
and might be a fruitful area for further investigation.) The doped carbonate
was calcined for $1100^{\circ}C$ for 1 hour to provide an average particle size of
300 $\overset{o}{A}$. These powders were consolidated under the same conditions as previously
employed for the high purity undoped materials.

A typical microstructure for a Ca-doped sample is compared with
that for a high purity $CaCO_3$ in Figure 12. The sample containing CaO has
smaller grain size than the undoped sample (Figure 12b) and also the
moderate-purity samples consolidated from the Honeywell M-10 material. All
microstructures are otherwise similar. This suggests that the Ca acted
as impurity drag on grain boundaries during the final stages of consolidation.

No evidence for a second phase could be obtained in the Ca-doped
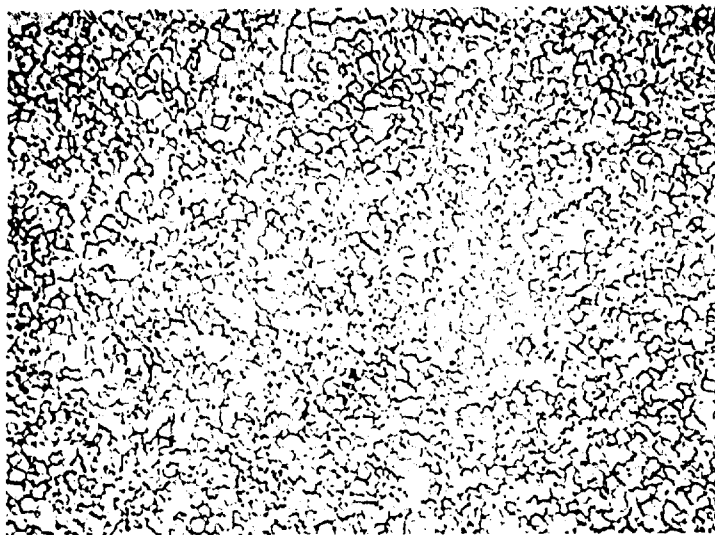
Baker MgO $\longrightarrow$ MgCO$_3$ $\longrightarrow$ MgO + 0.5 mole % CaO
Static calcine 1100°C - 1 hr.

Hot Pressed

1250°C - 15 Kpsi - 90 min.
3.580 gm/cc - 2.9 μm
grain intercept

#5525-1   (a)   500X

SH182 Mg(OH)$_2$ $\longrightarrow$ MgCO$_3$ $\longrightarrow$ MgO
Static calcined 1100°C - 1 hr.

Hot Pressed

1250°C - 15 Kpsi - 90 min.
3.566 gm/cc - 3.4 μm
grain intercept

#5525-3   (b)   500X

Figure 12. Comparison of Microstructures Produced with MgO Particulates Derived from (a) Mg$_{0.995}$Ca$_{0.005}$O Prepared by Co-precipitation and (b) High Purity Undoped MgCO$_3$.

microstructures with light microscopy. The specimens were therefore
fractured, and examined with replica electron microscopy. Figure 13a
indicates that the microstructure is uniform, and that the grains are equiaxed.
This is taken as evidence that the dopant was indeed uniformly dispersed
as intended. Some indication of the presence of a second phase is provided
by Figure 13a and a micrograph of one of these areas is presented at higher
magnification in Figure 13b. Discreet islands of second phase (arrow A)
appear on what is apparently a grain face. This would suggest that the
second phase is non-wetting. However, grain boundaries which are approximately
normal to this grain face (arrow B) appear to show a wide, continuous grain
boundary phase. A dihedral angle of 65° was estimated from a triple-point
intersection (arrow C). This is indicative of a partially-penetrating second
phase, which is consistent with the observation of second-phase islands on
grain faces.

Undoped MgO specimens were examined by identical techniques.
These provided no evidence of a second phase, and it is clear that the second
phase arises from the Ca dopant. Calcium oxide has limited solid solubility
in MgO, and limits of 3.5%, 1.1% and 0.9% have been established at 2015,
1820 and 1620°C, respectively.[15] Extrapolation to 1250°C, the processing
temperature of the microstructures of Figures 12 and 13 provides a
solubility limit of approximately 0.6% CaO. The concentration of dopant
should thus be within the range of solid solubility. Similarly, on the
basis of the diffusion coefficient for Ca^{2+} in MgO[8], distribution of a thin
film of CaO on the surface of a 3 micron sphere should be 95% complete
under the processing conditions. Since the initial particle size was 0.03
micron and the final grain size is 4.5 micron, it is clear that diffusion is
not rate limiting and the cause of the grain boundary phase. Only a few
speculative explanations seem possible: 1. A non-uniform distribution
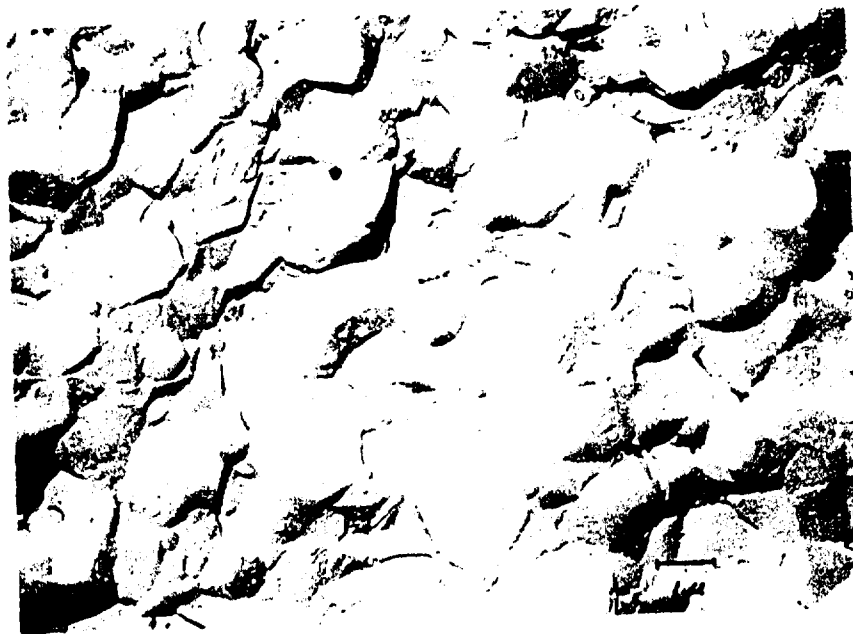
#71515   (a)   7500X
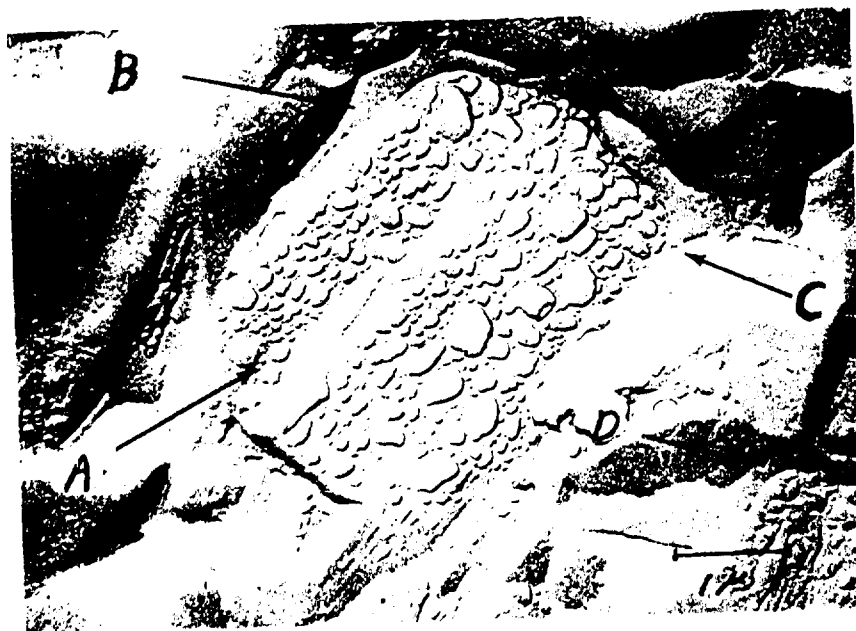
#71517   (b)   15,000X

Figure 14.   Fractographs of ThO₂.99/UO₂.01 O Microstructures
              Showing (a) Uniform, Equiaxed Microstructure and
              (b) Second Phase at Grain Boundaries.

of Ca in the initial particles causing local precipitation of CaO. The
reason which these precipitates should not be resorbed during processing is
not clear. 2. Reaction of CaO with another impurity, say SiO_2 to give a
different precipitate than CaO or, 3. A high segregation coefficient
resulting in precipitation of the (ant at the boundary even though it is
within the solubility limit. The last explanation seems likely inasmuch
as Leipold[1] has demonstrated boundary segregation - and for Ca^{2+} and Si^{4+}.
in particular - in MgO for impurities in bulk concentrations as low as 30
ppm.

3.2.6 Scale-up of Pressing Procedures

The 1" diameter pressings used for the studies of consolidation
and microstructure evolution provided sufficient material for examination
of further properties such as grain growth. The study of mechanical properties
to be conducted with the high purity material, however, required a large
number (ca 50) of 0.075 x 0.125 x 1.25 inch test bars which had to have
identical microstructures if sample-to-sample comparison of results were to
be possible. For this reason it was decided to scale up the pressing
conditions to produce a four-inch diameter billet from which the entire set
of identical test bars might be produced. The automatic rotary calciner
was used to produce a large volume of powder. The high purity carbonate
precursor was used exclusively for this purpose.

Difficulties were encountered in the scale-up procedure. Micro-
structures were encountered which were not comparable to those obtained
in one-inch diameter pressings primarily because of a lower pressure limit
(5 versus 15 kpsi) dictated by the use of a lower-strength large-diameter
graphite die. The resulting microstructuers displayed patches of large
grains which grew rapidly because of the high purity of the specimens.

Figure 14a presents a microstructure with 99.9% theoretical density which displayed this effect to a serious degree.

A considerable effort was directed toward re-establishing optimum pressing conditions for the scaled-up billets. In order to conserve the ultra-high purity carbonate, as well as to avoid the preferable, but time consuming rotary calcination, test runs were conducted with statically-calcined carbonate, and also with a lower purity Fisher $Mg(CO_3)$. Alternative processing techniques such as cold pressing and press forging were also briefly examined.

One alternative would have been to procure a high-strength, large diameter graphite die which would have permitted replication of the conditions of 15 kpsi and 1250°C at which fabrication of the one-inch diameter pressings had been optimized. We instead modified the time-temperature cycle at 5 kpsi to crease a slightly lower density. The small amount of retained porosity served to retard grain growth, and lead to an acceptable grain size distribution with a density of 99.6% theoretical. A typical microstructure in a four-inch diameter billet prepared under this approach is presented in Figure 15. Samples with this microstructure were subsequently machined into test bars for measurements of delayed fracture.

3.2.7 Isothermal Grain Growth

For normal grain growth in a pure, fully dense system, a theory due to Turnbull[16] predicts

$$D^2 - D_o^2 = (K \gamma V) t$$

where D is average grain diameter, D_o is initial grain diameter, K is a rate constant, γ is interfacial energy, V is molar volume, and t is time. In non-ideal systems either the migration rate of pores[17,18], the diffusion of impurities[19] ("impurity drag") or precipitation of a second phase[20]

(c)

may control grain growth kinetics. Brook[21] has considered the microstructural conditions for which each effect might be expected to be dominant. His results show that control by boundary mobility is to be expected when pores are small. Separation of boundaries from pores (pore entrapment) is to be expected when the pore velocity becomes less than the boundary velocity and will occur at large grain sizes and when the pores are large and widely dispersed. Porosity-controlled grain growth occurs at small grain sizes and when the pores are large and close together. The effect of impurity is to decrease the mobility of pores relative to that of the boundary and thus, for a given grain size, increase the boundary controlled region of behavior at the expense of the pore-entrapment region.

Several studies of grain growth in magnesia have been reported, but the influence of porosity and impurity on the process is not clear. Measurements by Daniels et al[4] were among the first to be conducted on a ceramic oxide. The data indicated normal grain growth, but the measurements were complicated by the presence of considerable porosity and attendant densification during grain growth. Spriggs et al[5] performed the first measurements with a fully dense material, but not of especially high purity. The kinetics of normal grain growth were again observed but, in the absence of porosity, growth rates were 4 to 6 times more rapid. Additions of 1% Fe or Ti impurity to magnesia[6] reduced growth rates to levels much smaller than those observed in either the porous[4] or fully dense microstructures,[5] and caused a change in the time dependence of grain diameter to 1/4 and 1/3 in the case of Fe and Ti additions, respectively.

Grain growth measurements in the present study were conducted with microstructures produced from $Mg(OH)_2$-derived powders which had been consolidated under processing conditons (Section 3.2.1) which produced a normal grain size distribution. The initial grain intercept for materials

hot pressed under these conditions was large (34.2 micron) which thus limited experiments to relatively high temperatures (above 1500°C) where measurable grain growth could be achieved in reasonable times.

Specimens were cut from a single pressing, polished and etched. A particular location in the sample was mapped, and grain intercepts were measured. The specimens were then placed in a closed high purity Al_2O_3 crucible, and in contact with a setter plate of the same high purity magnesia used in the study. Samples were inserted into a furnace in an air atmosphere and withdrawn after a prescribed time. After grinding to remove any surface effects, the samples were repolished and etched. Final grain sizes. reported as average grain intercepts, were measured in the same location in which the initial grain diameter had been measured.

The microstructures were carefully examined after annealing to determine the location and size of pores. Figure 16 illustrates the micro-structures which resulted from 1000 minute annealings at 1300. 1525 and 1610°C. These are to be compared with the starting microstructure typified by Figure 7c. It is clear that the pore level increases with increasing annealing tempera-ture. The pores are, in general. located at grain boundaries. However, a number of pores have separated from the boundaries and are located within grains.

Midway through the first year of this program an extensive study of grain growth kinetics in MgO was reported by Gordon et al.[22] This study had objectives similar to those planned for the present work. and included study of both pure and Fe_2O_3-doped MgO. The results of this work may be summarized as follows: (a) Very small amounts of porosity (0.1 to 0.8%) have a profound effect on grain growth in the temperature range $1300-1500^{\circ}$C. and pore control governed microstructure development in
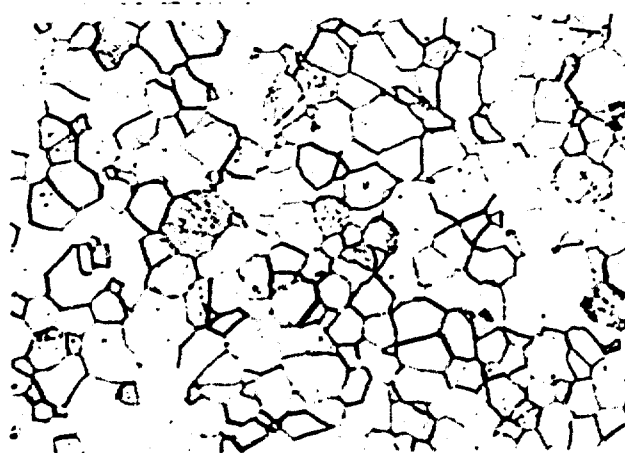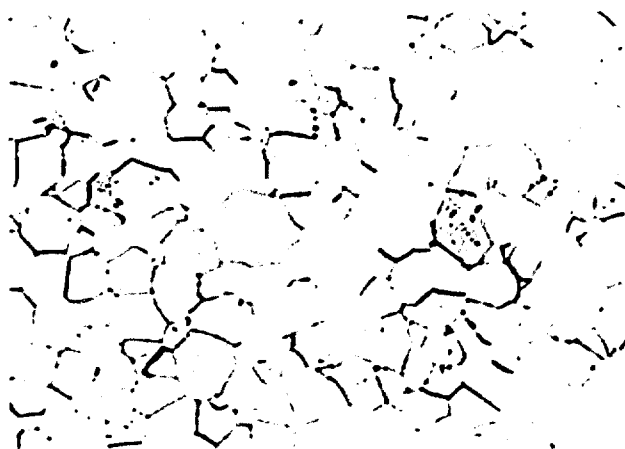
Figure 16. Microstructure of Mg(OH)$_2$-Derived MgO, with 34.2 Micron Initial Grain Size, after Heat Treatment for 1000 Minutes at (a) 1300°C, (b) 1525°C and (c) 1610°C.

all undoped samples. (b) Fe_2O_3 dopant stabilized squared kinetics at 1300°C, and decreased the growth rates at all temperatures.

The grain growth rates at all temperatures are compared with those of Gordon et al[22] and earlier work of Spriggs et al[5] in Figure 17. The present results exhibit a marked decay in growth rate with increasing time. (Plotting the data for other time-exponents n, in the relation $D^n - D_o^n = kt$ for values of n up to 4 could not fit all of the results, although the fit was moderately good at n = 4). The results are quite similar to those obtained by Gordon et al. The decay in growth kinetics occurred at different grain sizes at the different temperatures. The change in growth kinetics are likely to change from square to cube dependence as the controlling process changes from boundary to pore control.[21] Further decay beyond n = 3 will occur when pore entrapment occurs,[22] and the microstructures of Figure 16 indeed provide evidence for such entrapment. Pore separation apparently leads to abnormal grain growth as witnessed by the disproportionate number of grains in Figure 16 which have greater or fewer sides than the ideal number (6). This may occur because the pores become disassociated from individual boundaries non-uniformly - breaking away first from one boundary and then another. As pores break away from a boundary, that boundary becomes free to migrate at a faster rate than boundaries that are still bound to pores. This could lead to the development of 7 or more sides on a grain and the onset of abnormal grain growth.

The development of 0.1 to 0.5% porosity is quite common in hot pressed material upon annealing, and is thought to arise from either expansion of micropores contained under the load during hot pressing or coalescence of gas molecules adsorbed at grain boundaries. The present work as well as that of Gordon et al, shows that porosity of this level is sufficient to control grain growth kinetics. It is of interest to note
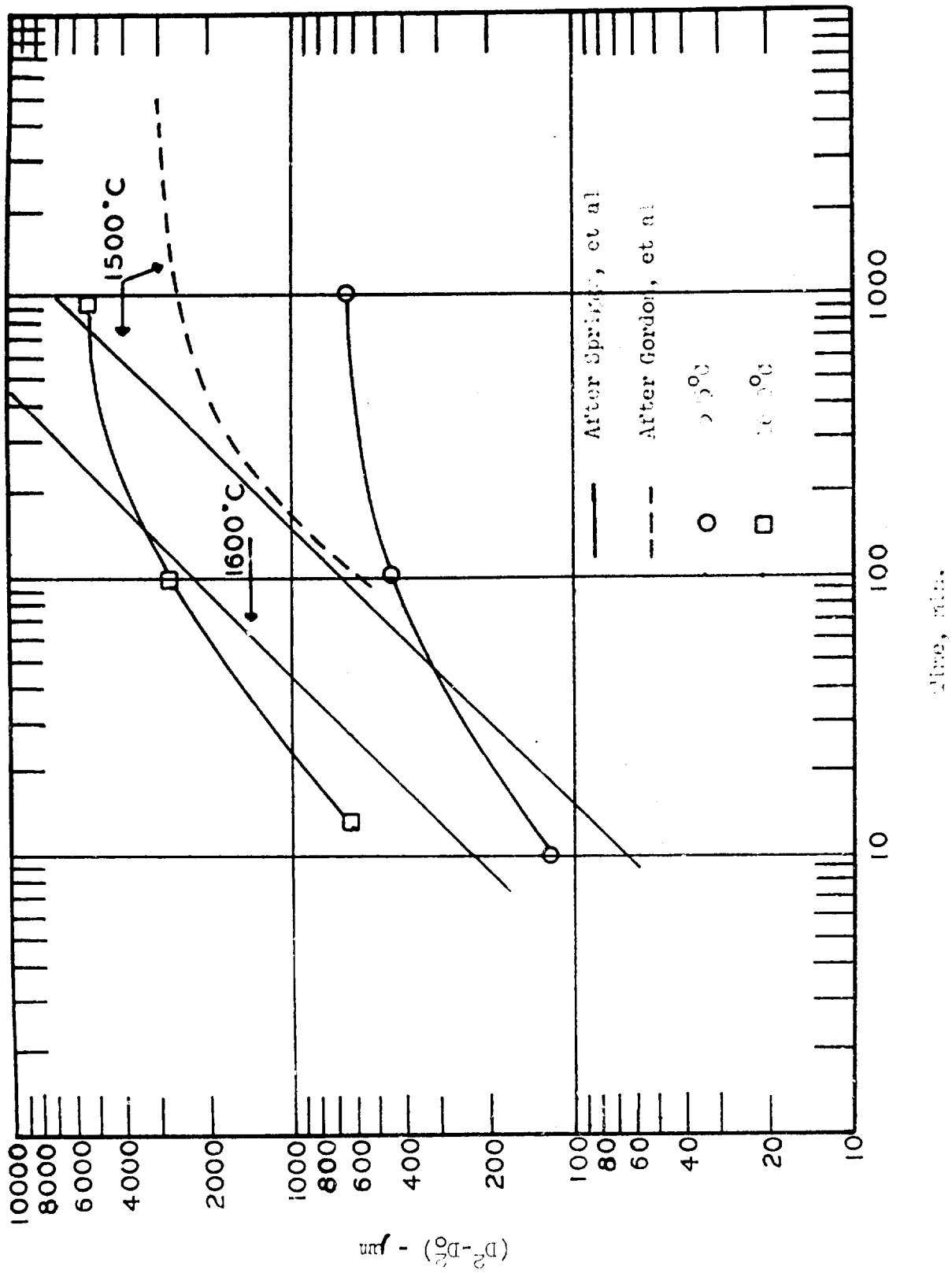
Figure 17. Grain Growth in High Purity Li_2O and Comparison with Literature Value.

that the initial growth rate observed in the present study is somewhat higher than that observed in previous work.[5] This may represent a decrease of impurity drag in an initial boundary-controlled regime for this higher-purity material. Since the data obtained in this study appeared to confirm the recent findings of Gordon et al[22] study of grain growth kinetics received less emphasis in this program than originally intended.

3.3 Delayed Fracture in High Purity MgO

3.3.1 Introduction

Magnesium oxide is one of the few materials investigated to date in which it has been shown that grain boundary impurities play a role in stress corrosion.[23] Stress corrosion cracking is a well known phenomena that may be controlled by either mechanical or chemical processes occurring at the interface between a solid and an environment. In most cases the surface interaction degrades the usable strength and, consequently, under-standing of such reactions is important for structural materials.

There are two major classes of models governing the advancement of the stress corrosion crack: (1) Those which postulate crack advancement by stress-enhanced chemical dissolution at the crack tip, and (2) Those which involve only mechanical effects such as mobile dislocations or the reduction of the surface energy term in the Griffith relationship. Previous studies which have been conducted with MgO, and the evidence for chemical as opposed to mechanical mechanisms are summarized in detail in Appendix B.

3.3.2 Results

Dead-load delayed fracture tests were performed in three different environments in an attempt to distinguish between mechanisms involving stress-enhanced chemical dissolution at crack tips and processes involving enhanced dislocation mobility. Water was selected as one environment. The other involved two complexes of high charge: DMF (I.M. dimethyl formomide

$(CH_3)_2$ NCHO) and a mixture of DMSO-DMF $((CH_3)_2SO$ - 10 vol. % $(CH_3)_2$NCHO).
Dislocation velocities in MgO have been shown to be a minimum in the DMSO-
DMF system for the latter composition. The time-to-failure was measured at
room temperature as a function of relative stress, σ / σ_o, where σ_o,
the dry strength, was found to be 21.6 $\pm$ 1.5 kpsi, and compared with
corresponding data which had been obtained for three very different grades
of magnesia: Ambient hot pressed 99.6% MgO, vacuum hot pressed 99.6 MgO
+ 1.6% LiF and sintered MgO of high purity.

The results show that the ultra-pure MgO produced in the present
study displays notably increased resistance to delayed failure compared to
other grades of material of lesser purity. The time-to-failure at any
stress level is increased as the purity of the material increases. Unlike
the less-pure materials, the time-to-failure of ultrapure MgO is identical
in both H_2O and DMF, even though dislocation mobilities are seven times
higher in the latter medium.

A detailed discussion of experimental procedures and results is
attached as Appendix B.

IV. CONCLUSIONS

1. Brucite decomposes by the coherent nucleation of MgO leaving
crystallographically oriented MgO crystallites within an agglomerate which
is a relic of the parent $Mg(OH)_2$ crystal. Preferred growth directions
resulted in a rod-structure when calcination was conducted at 375°C. and
cubic particles when calcined at 900°C and above.

2. Magnesium oxide derived from $MgCO_3$ also possesses cubic
particles, but they are unoriented with respect to one another within
agglomerates.

3. Marked duplex microstructures developed in hot pressed MgO
which is derived from brucite. This microstructure persists in both

statically or dynamically calcined material, and evolves early (at less
than 70% density) in the densification cycle.

4. Vacuum hot pressed bodies derived from $MgCO_3$ have normal grain
size distributions and average grain sizes which are 30 times smaller
than those obtained with microstructures derived from a hydroxide. The
difference in microstructures does not lie in subtle differences in purity
as demonstrated by the development of equivalent results upon the conversion
of one precursor to another.

5. The marked differences in microstructure which may be obtained
from different precursors of similar high purity is attributed to the
physical state of the agglomerated particles in the hydroxide-derived
powders. In the absence of significant impurity, the high degree of
mutual orientation is believed to create a highly-mobile boundary which can
rapidly sweep through an agglomerate and provide a nucleus for secondary
grain growth.

6. Adsorbed volatiles such as OH^- or CO_3^{2-} were found to have
little influence on microstructure development in a 99.96% pure MgO
derived from $MgCO_3$.

7. Freeze-dried $MgCO_3$ cannot be easily obtained, but use of
acetates appears promising. Calcia-doped $MgCO_3$ was readily prepared
through coprecipitation.

8. Calcia-doped MgO ($MgO_{.995}Ca_{0.005}$) was consolidated to dense,
equiaxed microstructures. Grain sizes were smaller than those obtained
from high-purity material under similar conditions. Evidence was found
for a partially-penetrating second phase at grain boundaries. The amount
of second phase seems excessive based upon known solubility limits for
CaO in MgO, and on the diffusion rates operative during processing.

9. Grain growth rates at 1526°C and 1610°C decrease rapidly with time due to a transition from boundary control to pore control to abnormal grain growth.

10. High purity microstructures produced from carbonate-derived powders displayed higher resistance to stress-corrosion cracking and a higher static fatigue limit than any other grade of less pure material which was examined.

V. REFERENCES

1. M.H. Leipold, J. Am. Ceram. Soc., 49, 498 (1966).

2. B.J. Wuensch and T. Vasilos, J. Am. Ceram. Soc., 49, 433 (1966).

3. R.J. Stokes, J. Am. Ceram. Soc., 48, 60 (1965).

4. A.U. Daniels, Jr., R.C. Lowrie, Jr., R.L. Gibby and I. Cutler, J. Am. Ceram. Soc., 45, 282 (1962).

5. R.M. Spriggs, L.A. Brissette and T. Vasilos, J. Am. Ceram. Soc., 47, 417 (1964).

6. G.C. Nicholson, J. Am. Ceram. Soc., 49, 47 (1966).

7. W.H. Rhodes and R.M. Cannon, "Microstructure Studies of Refractory Polycrystalline Oxides," Summary Report, Contract N00019-69-C-0198, December 1969.

8. Available data are summarized in: B.J. Wuensch and T. Vasilos, N.B.S. Spec. Publ. 296, 95 (1968) and B.J. Wuensch, W.C. Steele and T. Vasilos, J. Chem. Phys. (June 1973) in press.

9. R.S. Gordon and W.D. Kingery, J. Am. Ceram. Soc., 49, 654 (1966).

10. Y. Oishi and W.D. Kingery. J. Chem. Phys., 33, 905 (1960).

11. F.J. Schnettles, F.R. Montforte and W.W. Rhodes, Science of Ceramics, 4, 79 (1968).

12. D.W. Johnson and F.J. Schnettler, J. Am. Ceram. Soc., 53, 440 (1970).

13. S.M. Copley and J.A. Pask, J. Am. Ceram. Soc., 48, 636 (1965).

14. R.W. Rice, Proc. Brit. Ceram. Soc., 99, (1969).

V. REFERENCES (Concl'd)

15. R.C. Doman, J.B. Barr, R.N. McNally and A.M. Alper, J. Am. Ceram. Soc., 46, 313 (1963).

16. D. Turnbull, Trans. A.I.M.E., 191, 661 (1951).

17. W.D. Kingery and B. Francois, J. Am. Ceram. Soc., 48, 546 (1965).

18. F.A. Nichols, J. Appl. Phys., 37, 4599 (1966).

19. J.W. Cahn, Acta. Met., 10, 789 (1962).

20. M. Hillert, Acta Met., 13, 227 (1965).

21. R.J. Brook, J. Am. Ceram. Soc., 52, 56 (1969).

22. R.S. Gordon, D.D. Marchant and G.W. Hollenberg, J. Am. Ceram. Soc., 53, 399 (1970).

23. W.H. Rhodes and R.M. Cannon, "Microstructure Studies of Refractory Polycrystalline Oxides," Contract N00019-70-C-0171, February 1971.

24. A.R. Westwood, D.L. Goldheim and R.G. Ive, Phil. Mag., 16, 505 (1967).

APPENDIX A

A RELATIONSHIP BETWEEN PRECURSOR AND MICROSTRUCTURE IN MgO

(Submitted to Journal of the American Ceramic Society)

A RELATION BETWEEN PRECURSOR AND MICROSTRUCTURE IN MgO

W.H. Rhodes and B.J. Wuensch

The final consolidated microstructure of a ceramic body is dependent
not only upon its thermal history, but also upon the initial state of
particle agglomeration and the influence of impurity drag on grain growth.
In the course of an effort to develop a fine-grained, high-purity MgO
through pressure sintering, it was discovered that the precursor from which
a powder is derived may also have a profound effect on microstructure
evolution during consolidation.

The decomposition of brucite, $Mg(OH)_2$, which was nominally 99.9995%
pure*, was followed with transmission electron microscopy. Under the
influence of heating by the electron beam, the intensity of the hk.0
brucite diffraction pattern gradually diminished with time. The (220)
reflection of MgO appeared along the 11.0 reciprocal lattice vector of
brucite initially at a position corresponding to a larger-than-normal
lattice constant, but gradually shifted to its expected position. The
cubic MgO crystallites thus develop with $\{110\}$ and $\{111\}$ parallel to the
prism and basal planes, respectively, of the parent hexagonal $Mg(OH)_2$ plate.
This is in accord with the observations of Gordon and Kingery[1] who describe
the process as a nucleation and growth mechanism in which MgO nuclei form
coherently with the brucite matrix. Large strains are introduced which
result in eventual fracture of the brucite plate. Guilliatt and Brett[2]
found the MgO crystallites to be better described as octahedra whose size
was related to the initial thickness of the $Mg(OH)_2$ plate.

Powders in volume sufficient for consolidation were produced in the

present work through calcination of brucite in 1 torr vacuum. Initial

calcinations were conducted at low temperatures (350° to 800°C) with the

precursor loosely packed to a depth of 2 mm. Cubic MgO crystallites of

sizes ranging from 100 to 360 Å were produced which were highly oriented

within a relic of the parent brucite plate. Prolonged heat treatment

(ca. 3 hrs.) produced an oriented rod-like MgO product. Rotary calcination

was employed in subsequent production in an attempt to break down the relics.

Further, to eliminate the possible effect of small amounts of retained

hydroxyl on microstructure development (discussed below) calcination temper-

atures were employed (800° to 1200°C) which were far in excess of those

necessary to decompose brucite. This procedure destroyed the plate-like

relics, and any indication of a preferred growth direction in the magnesia

crystallites. The product, Figure 1a, consisted of smaller agglomerates

of particles with cube-like morphology, but which retained a high degree

of mutual orientation.

The particles produced through rotary vacuum decomposition of high-

purity brucite were consolidated to between 99.4% and 100% theoretical

density through vacuum hot pressing at temperatures between 1150° and 1250°C

and times between 30 and 180 minutes under an applied pressure of 15 kpsi.

Invariably, a marked duplex grain structure resulted, as illustrated in

Figure 1b. This structure was found to evolve early in the course of

consolidation, at as little as 70% theoretical density.

Pressure sintering experiments which employed MgO derived from reagent-

grade $MgCO_3$ were also conducted. It was noted that a normal grain size

distribution was obtained in the final microstructure. Moreover, the average

grain size was up to a factor of 10 smaller than the large grains of Figure

1b after equivalent thermal cycles. It was initially felt that impurities in

this less pure powder might have stabilized grain growth. However,

identical microstructures were obtained when 99.999% MgCO₃** was calcined

and pressure sintered. Finally, to completely eliminate differing impurity

contents as the source of the exaggerated grain growth in the brucite-

derived magnesia, the brucite was carefully converted in $MgCO_3$ by dissolution

in HNO_3, and precipitation of the carbonate through addition of NH_4CO_3.

This high purity carbonate was statically calcined at $1100^{\circ}C$ for 1 hour,

and pressure sintered at the same temperature as the $Mg(OH)_2$-derived micro-

structure. The resulting microstructure, depicted in Figure 1d, had a

normal grain size distribution. The 3.4 µm grain intercept (compared with

16 µm for Figure 1b) is noteworthy. Three grades of $MgCO_3$, ranging from

moderate to very high purity, thus gave identical normal grain size distribu-

tions in the final microstructure. This strongly suggested that the differ-

ent behavior of the brucite-derived material arose from the physical, rather

than the chemical nature of the initial MgO particulates.

$MgCO_3$ undergoes a 60% reduction in molal volume upon conversion to

MgO, as opposed to 55% for $Mg(OH)_2$. Although the decomposition mechanism

and kinetics have not been thoroughly investigated for the carbonate, the

larger molal reduction may result in more displacement between crystallites.

The cube-shaped particles, while agglomerated (Figure 1c), were indeed

found to be more randomly oriented to one another, which suggests that

coherent nucleation of the MgO is unlikely.

A plausible explanation for these microstructure-precursor relation-

ships lies in the high degree of crystallographic orientation within

agglomerates of the MgO crystallites produced from $Mg(OH)_2$. The primary

surfaces in the latter material are $\{100\}$ and each crystallite is aligned

parallel to a neighbor in identical orientation. As sintering and grain

---

**Johnson-Mathey Co.

growth commence during the densification cycle, these oriented faces are believed to become coherent grain boundaries which migrate at a much faster rate than interfaces between randomly oriented crystallites which broke away from their parent agglomerate during some stage of processing. (Rapid migration of boundaries in high-purity materials is well known in the metallurgical literature, and growth rates of the order of mm/min. have been reported[3,4]. Such rates are especially high for coincidence boundaries.[4] Once the coherent boundaries have swept through them, the agglomerates become nuclei for exaggerated grain growth near the end of the intermediate stage of sintering and, having formed, dominate development of the final microstructure. Although agglomerates exist within the $MgCO_3$-derived powder, the random orientation of crystallites would suppress rapid intra-agglomerate grain growth. The high purity of the $Mg(OH)_2$-derived magnesia may also be a requisite for the development of large grains since impurity drag could limit the enhanced mobility of the boundaries. It is of interest to note that the fine grained patch in Figure 1b has about the same grain size as the microstructure of Figure 1d, which lends support to the proposed model.

Acknowledgment

References

1. R.S. Gordon and W.D. Kingery, "Thermal Decomposition of Brucite: I, Electron and Optical Microscope Studies," J. Am. Ceram. Soc., 49, 12, 654-660 (1966).

2. I.F. Guilliatt and N.H. Brett, "Crystallite Size and Shape Relationships in the Product-Precursor Pair MgO-$Mg(OH)_2$," Phil. Mag., 23, 183, 647-652 (1971).

3. J.W. Rutter and K.T. Aust, "Grain Boundary Migration Motivated by Substructure in High Purity Metal Crystals," Acta. Met., 6, (5), 375-377 (1958).

55   ⋮   -5-

4. a) K.T. Aust and J.W. Rutter, "Grain Boundary Migration in High
        Purity Lead and Dilute Lead-Tin Alloys," Trans. Met. Soc. AIME,
        215 (1), 119-127 (1959).

    b) K.T. Aust and J.W. Rutter, "Temperature Dependence of Grain
        Migration in High-Purity Lead Containing Small Additions of
        Tin," Trans. Met. Soc., AIME, 215, (5), 820-831 (1959).

Figure Caption

Figure 1   Precursor Product-Microstructure Relationships

(a) MgO derived from $Mg(OH)_2$ by rotary vacuum calcination,
     $1200^{\circ}C$, 1 hr. Note high degree of mutual orientation
     of crystallites within agglomerates.

(b) Microstructure produced from powder shown in (a)
     through vacuum hot pressing for 30 min. at $1250^{\circ}C$
     under 15 kpsi, 15 μm grain intercept, 99.9% theoretical
     density.

(c) MgO derived from $MgCO_3$ converted from the $Mg(OH)_2$
     employed in (a). Static vacuum calcination, $1100^{\circ}C$,
     1 hr.

(d) Microstructure produced from powder shown in (c)
     through vacuum hot pressing for 90 min. at $1250^{\circ}C$
     under 15 kpsi, 3.4 μm grain intercept, 99.4%
     theoretical density.
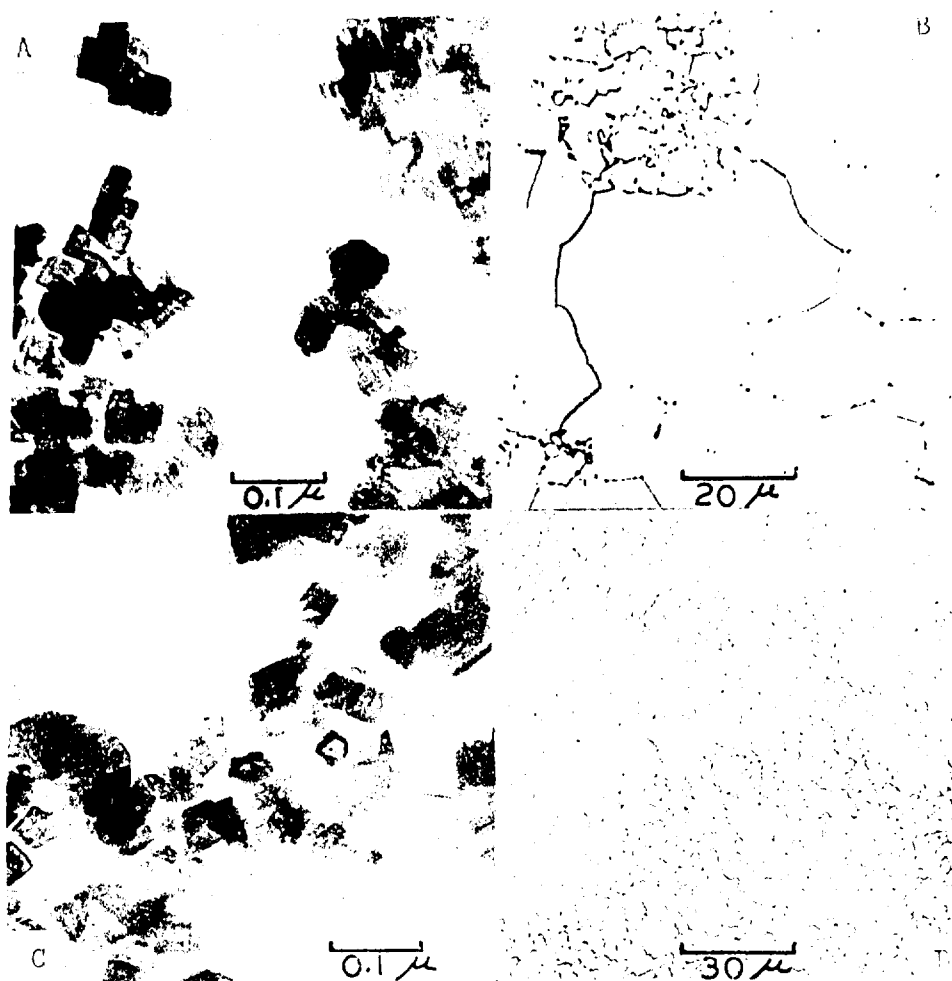
APPENDIX B

STRESS CORROSION CRACKING IN POLYCRYSTALLINE MgO

(To appear in Proceedings of the Symposium, "Fracture Mechanics of Ceramics," University Park. Pa., July 11-13, 1973)

STRESS-CORROSION CRACKING IN POLYCRYSTALLINE MgO

by

W.H. Rhodes and T. Vasilos
AVCO SYSTEMS DIVISION
Lowell, Massachusetts 01851

ABSTRACT

Stress-corrosion cracking (SCC) was studied in four grades of $99^{+}\%$ dense MgO with the major variables grain size and purity. Testing consisted of 4-point bend and static fatigue tests in H_2O, DMF, and DMSO-DMF solutions. In a H_2O environment the highest purity material gave the slowest corrosion rates. SCC in low purity grades was judged to be controlled by a chemical interaction of OH^- with a $(CaNaSiAl)O_x$ grain boundary phase. The highest purity grade tested ($99.98^{+}\%$ MgO) may not have a discrete grain boundary phase, so the low corrosion rate and high static fatigue limit of $\cong 0.83\,\sigma_D$ may be characteristic of an intrinsic process. The possibility exists that this was due to a shift in mechanism, but a passive film model consistent with the data is proposed. When H_2O is present, chemical corrosion is believed to have faster SCC kinetics than possible competing processes. This was demonstrated for the second purest ($99.92^{+}\%$ MgO) specimens. Testing in DMSO + 10% DMF and DMF gave a sufficient separation of the data to conclude that the Rebinder effect was operative. Thus, under certain conditions, SCC can result from a dislocation model of crack nucleation. Stress intensity factors, K, were calculated based on the conclusion that the Griffith model was operative. The calculated K-V (velocity) diagram was thought to be qualitatively correct in showing that the second purest sintered grade of MgO had the best overall behavior in terms of dry strength and static fatigue in a H_2O environment. However, the static fatigue performance and nearly identical K_{ISCC} for the highest purity material suggested that the high purity hot pressed grade showed the most promise from a materials development viewpoint.

I. INTRODUCTION

Crack propagation by stress corrosion is a frequently encountered phenomena in the structural application of materials. Allowable long time loads in ceramics are dictated then not only by the dynamic strength, standard deviation, and application of the Weibull parameters to the volume under load, but knowledge of the static fatigue limit (stress below which failure does not occur at infinite times) for the material and perhaps grade of material under question. Among ceramics materials silicate glasses have been most extensively studied[1-4] with the general conclusion that a chemical

60

-2-

corrosion model applies although some question remains[5] as to whether the
Charles and Hillig[6] stress dependent chemical reaction between water and a
pre-existing flaw theory, the Cox[7] atomistic weakening theory, or the ion
exchange theory[8] applies. Alumina is the crystalline ceramic most extensive-
ly studied[9-11] with investigators initially proposing fatigue being due to
chemical processes[12], as alumina was thought to behave in a completely
brittle manner, and more recently[9,13] suggestions based on static and cyclic
fatigue results indicate that dislocation motion and crack tip lattice
defect creation are likely causes of failure.

Few static fatigue tests have been performed on MgO, which is surprising
since it has served as a model system for the examination of mechanical
phenomena in ceramics. Charles[14] performed dynamic $240^{\circ}C$ compressive tests
on single crystal MgO in saturated H_2O vapor and dry N_2 with resulting
failure stresses of 8 Kpsi and 26.6 Kpsi, respectively. Considering the
known hydration behavior of MgO, he speculated that a chemical stress corro-
sion model similar to glass applied. Janowski and Rossi[15] noted loss of
strength in polycrystalline MgO by water vapor attack with a similar inter-
pretation. In contrast, Rice[16] interpreted a loss of dynamic strength for
both single and polycrystalline MgO tested in H_2O to be a result of enhanced
dislocation mobility by the Rebinder effect. A number of models have been
proposed to explain the Rebinder effect[17], which basically applies to
absorption-induced reductions in hardness or enhanced dislocation mobilities.
Westwood et al[17] measured slight increases in dislocation mobility for the
H_2O environment compared to ambient, and further enhancements by a factor of
4 in dimethyl formamide (DMF), a high dipole moment organic molecule. They
proposed that the observed Rebinder effect was due to chemisorption-induced
bond bending which altered the electronic core structure of near surface

dislocations and point defects and consequently the resistance of the lattice to dislocation flow. Shockey and Groves[18] concluded that the increased fracture surface energy in H_2O as measured by the double cantilever method was due to increased surface roughness due to a change in the fracture plane perhaps imposed by a chemically altered surface layer. Measurements in DMF failed to show any enhanced toughening due to higher dislocation mobilities.

Clear evidence has been generated for a dislocation mechanism of crack nucleation in single crystal MgO[19,20]. Debates continue, however, between investigators[16,21-24] on the mechanism of dynamic fracture under ambient conditions in polycrystalline MgO. On one hand, fracture can be caused by the fulfillment of the Griffith criteria on the elastic propagation of existing flaws, or alternatively mobile dislocations can interact with other defects[18] or structural features[20,24] to nucleate a critical crack. The answer probably lies in between with the mechanism dependent on the surface condition and lattice hardness, e.g., elastic extension of cracks for machined surfaces and Stroh model[25] dislocation initiated fracture on chemically polished surfaces.[24] Further, Rice[16] has shown that increased strengths are observed for specimens which experienced slow annealing which apparently distilled off impurities The mechanical behavior of polycrystalline MgO is obviously very complex and not subject to simple analysis, but the vast background available offers an opportunity to study phenomena that may occur in many systems.

A major goal of this study was to define the level of stress-corrosion cracking, SCC, for dense polycrystalline MgO not only to indicate the severity of the problem from a design viewpoint, but to determine if such measurements could further elucidate the mechanism of crack nucleation and/or propagation in polycrystalline MgO. A second major objective was to determine

if some material property such as microstructure or chemistry controlled the level of SCC.

II.   EXPERIMENTAL

A.   Materials

Testing was conducted on four grades of MgO spanning the range of commercially available electronic quality materials plus a high purity grade developed specifically for the purposes of these experiments. Preliminary testing suggested that a high purity material might be essential toward interpreting results. The latter material was vacuum hot pressed using MgO powder that was rotary calcined from 99.9998% $MgCO_3$. Table I describes the general character of the four materials tested. Grade II material was the highest quality sintered MgO available commercially and also the second purest grade. Grade III was ambient atmosphere hot pressed and Grade IV was optical grade MgO produced with a 5% LiF densification aid. A post pressing anneal of 60 hrs. at $1000^{o}C$ reduced the LiF content to 0.1%. In general, one large billet of each grade was employed for the program to eliminate the problem of sample to sample inhomogeneity. The problem of within-billet homogeneity was approached by dividing the billets into zones, and spreading specimens from each zone among the testing environments and conditions.

All specimens were tested with machined surfaces where the final operation was grinding with a 400 grit diamond wheel parallel to the long axis of the bar. The use of machined surfaces having an abundance of surface flaws was thought desirable to insure a surface fracture origin. The question of whether machining gave a work hardened layer preventing surface nucleated fracture was considered in the fractographic analysis. A 1/8-inch radius was machined on the two tensile edges to remove these stress concentrations.

TABLE I

Description of Materials

Grade	Method of Fabrication	Density % Theoretical	Grain Size, μm	Purity %	Major Impurities (in ppm W)
I	Vacuum Hot Press	99.6	46	99.98+	*100 Fe, 40 S, 30 Ca, 20 Al, 20 F
II	Sintered**	99.3	43	99.92	300 Si, 300 Na, 70 Al, 50 Ca, 50 Fe
III	Ambinet Hot Press	99.8	26	99.40	1500 Ca, 500 Fe, 750 Si, 100 Na, 150 Al
IV	Vacuum Hot Press	100	30	99.60	1000 Na, 750 Si, 800 Ca, 500 Li, 500 F

*Mass Spectroscopy - others by electron spectroscopy.
**Honeywell

The chemistry of Grade I was examined in detail by spark source mass spectroscopy and emission spectroscopy. The values reported in Table I are spark source numbers on the specimen employed in the testing program. The starting powder was analyzed by both techniques and the reported spark source numbers were 2-10 times higher than the emission spectrograph values, e.g., 30 ppm Ca by spark source spectroscopy and 3 ppm Ca by emission spectroscopy. This discrepancy in analytical techniques underestimates the difference in Grade I and Grade II. Grade I is probably 10 to 30 times purer than Grade II instead of the factor 4 indicated in Table I. The analytical comparison of the fabricated piece and powder for Grade I revealed that Fe was the only element introduced bringing the concentration from 30 ppmw to 100 ppmw. The analyses for the remaining grades are typical emission spectroscopy results not specifically of the specimens tested.

The microstructures for the four materials are illustrated in Figure 1. All of the structures are equiaxed. The grain sizes reported are the linear intercepts corrected for geometry by the factor 1.5. The strengths for each grade were normalized relative to that billet's dynamic dry strength, making it possible to test materials of different grain size, etc. In general, the porosity was located at a grain surface site. Grade IV had 82% total transmission confirming its low porosity while Grade III was transparent but to a lesser degree. The structure of the grain boundaries were examined by electron microscopy techniques on fracture surfaces (Figure 2). The fractographs for Grades II, III, and IV show an apparent 0.1 to 0.2 um width which is interpreted as being evidence for a grain boundary phase. Electron diffraction was performed on numerous "pull-off" particles on the Grade III replicas. Many of these were MgO as expected, but one pattern indexed as $Mg Al_2 Si_4 O_4$ which is taken as further evidence for discrete grain boundary

phases. Grade I, the highest purity material was examined by both replica and scanning electron microscopy and, although the boundaries appeared clean, it was unclear if they were completely free of a second phase. Secondary X-ray emission mapping was not productive, but integrated counting on a fracture surface demonstrated a high Ca concentration relative to that expected based on the bulk analysis. This was taken as evidence for Ca segregation at grain boundaries in Grade I material.

B. Test Technique

Base line dynamic strengths were established for the four grades by testing in corrosion-free environments. It is generally agreed that testing in liquid N_2 provides one such environment.[11,14] Since a mechanical model of fracture initiation was also being considered, it was important to consider the fact that the $\{110\}<110>$ yield stress increases by a factor of two[27] from $23^{\circ}C$ to $-196^{\circ}C$. Thus, on alternate base line strength, testing technique consisted of heating the sample to $900^{\circ}C$ in argon, holding for 1 hr., cooling to $23^{\circ}C$, and loading the specimen without altering the environment. Base line tests on Grade IV gave 209 MN/m^2 in liquid N_2 and 210 MN/m^2 in argon. The strengths were judged equivalent; however, base line strengths for the other grades were established by the bake-out argon test at a strain rate of 8×10^{-5} sec^{-1} and are designated, σ_D.

Long term tests were conducted in a lever arm test frame equipped with a microswitch to record time to failure at a given stress. A brass 4-point bend test fixture was equipped for holding liquids. Tungsten (outer) and alumina (inner) knife edges employed a thin mylar sheet to give separation from the test bar. This precaution prevented chemical interactions even in the 1 to 4 week tests. Distilled H_2O was employed as a test environment that was judged mildly corrosive by the reaction

-8-

$$MgO + H_2O \longrightarrow Mg(OH)_2 \qquad\qquad (1)$$
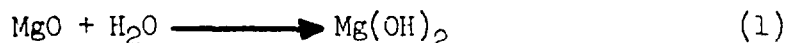
Testing on the effect of increasing dislocation mobility stress corrosion was performed in the environments employed by Westwood et al[17] in their classic dislocation mobility experiments on MgO. Dimethyl formamide (DMF), either pure or as 1 M DMF should enhance dislocation mobility by a factor of 6-7 over H_2O. A third testing environment was dimethyl sulphoxide (DMSO) plus 10% DMF which was shown to depress dislocation mobility over pure DMF to about the same level as H_2O; thus, in combination with the other environments, provided a separation of chemical and mechanical effects. Each sample was immersed for 1 hr. prior to loading to insure complete absorption and equilibration of surface and near surface charge effects. The loading and timing devices were constructed such that data was judged accurate for ≥ 2 sec.

III. RESULTS

A. Dynamic Tests

Dynamic bend strength measurements first raised the question of the importance and mechanism of stress-corrosion in MgO. A billet of Grade III material having a 6.5 μm grain size was tested in air and argon after a 900°C - 1 hr. outgas.[28] An average of four 8×10^{-5} sec^{-1} strain rate tests gave strengths of 298 MN/m^2 and 296 MN/m^2 for the two environments, respectively. This was in marked contrast to similar tests on Al_2O_3[28] where strength reductions of 20% were experienced for ambient tests.

Limited dynamic testing was performed on the billets for this study. Not only was it important to establish the "corrosion-free" strength, but the effect of the various liquid test environments on dynamic strength was determined. The average of 3-6 strength measurements for each condition is reported in Table II.

TABLE II

Dynamic Strength of MgO Specimens in Various Environments

	Four-Point Bend Strength, MN/m^2					
	Argon-After Anneal, σ_D	Liquid N_2	Ambient	H_2O	DMF	DMSO-10% DMF
Grade I 46 μm G.S.	149					
Grade II 43 μm G.S.	192			172	174	187
Grade III 26 μm G.S.	167					
Grade IV 30 μm G.S.	210	109	183			

The ambient tests on Grades III and IV are both lower than the argon tests, but the difference is within the $\sim \pm$ 20.7 MN/m^2 standard deviation for each test. Testing on Grade II was performed in liquid H_2O and again only slightly lower strengths were measured compared with the dry strength. Clearly, then, on the basis of dynamic tests, there was very weak evidence for the stress corrosion action of H_2O on MgO. Similar tests on other ceramics, notably Al_2O_3 and glass, would have clearly demonstrated the loss of strength due to stress-corrosion.

The tests of Grade II in DMF and DMSO-10% DMF gave results within the scatter of the dry strengths. Thus, no firm conclusions can be drawn concerning dynamic crack initiation and propagation. This is in contrast to the work of Westwood and Latanision[29] where drilling rate was affected by n-alcohol environments, and the results interpreted to be the result of the Rebinder effect. If the Rebinder effect required an incubation period or other time dependent processes, drilling would be expected to suppress the effect to a greater degree than a dynamic strength test. The strength results are

consistent with a portion of the Westwood et al[17] study on dislocation
mobility in single crystal MgO. They found that dislocation mobility after
2 sec of load application was insensitive to environment and only after a
longer 10 sec application were the Rebinder effects apparent. The dynamic
strength results appear to follow this type of behavior and it is quite
puzzling why drilling should be any different.

The σ_D values appear consistent with previous literature values on
MgO produced by similar processes and with similar microstructures. Leipold
and Nielsen[30] and Rice[16] noted lower strengths for the highest purity samples
after normalizing for microstructure effects. This was attributed to higher
dislocation mobility resulting from reduced Pierls stress which promoted
early dislocation nucleated fractures. The Grade II sintered specimens
might be expected to have slightly higher strengths than hot pressed speci-
mens of equivalent microstructure due to the expected reduction in anion
impurity concentration from the sintering cycle. This also explains the
higher strength of Grade IV compared with Grade III and Grade IV was annealed
in a slow heating rate cycle that has been shown by Rice[16] to reduce anion
concentration and increase strength.

B. Static Tests

Dead load tests in distilled H_2O are plotted in Figure 3 for
Grades I and II. Due to the large scatter which is typical of stress-
corrosion results, the data for Grades III and IV are plotted in Figure 4.
Also shown in Figure 4 are the straight lines for the best fit to the data
of Figure 3. Points highlighted with an arrow indicate a test discontinued
without failure. Such points were used in drawing the indicated lines with
a strong weighting factor if the point was above the general fit of the
data and lesser weight if the point was below the line. Grades II and III

to the environment prior to loading was employed. The data for this environment exhibited little scatter. However, due to the scatter of data in the other environments, it does not appear possible to draw conclusions regarding distinguishable behavior from one environment to the next for Grade I.

The data for Grade II, plotted in Figure 7, exhibits greater separation. The DMSO-10% DMF data falls midway between failure data in H_2O and DMF. Three orders of magnitude in time separate the expected failure times in H_2O and DMSO-10% DMF, and approximately one order of magnitude separate the DMF and the DMSO-10% DMF data. The significance of the seapration for the latter two environments may be argued, but the authors attach moderate significance to all three sets of data.

Grade IV was tested in more than one environment, and a comparison for the delayed failure in H_2O and 1M DMF is shown in Figure 8. This short time data in 1M DMF is quite interesting. Attempts to load above $\sigma / \sigma_D = 0.627$ in this environment resulted in immediate failure, thus the effect of 1M DMF is the reverse of that found for Grade II.

C. Fractography

Replica and scanning electron micrographic techniques were employed to examine the fracture surface near the tensile edge. Figure 9a illustrates a series of linear etch pits found in a Group II H_2O tested specimen which fractured after 1.2×10^6 sec. Another grain face of this specimen (closer to the tensile surface) also showed etch pits, but with an apparent random crystallographic orientation and flat bottoms, Figure 9b. The linear pit lines are interpreted to correspond to arrest points of the crack front. The randomness of the pattern on Figure 9b and the apparent flat bottoms argue against their being associated with dislocations. Thus, the interpretation is that chemical corrosion generates the pits with increased

activity at regions of stress concentration. A Group IV specimen also fractured in H_2O after 6.8×10^3 sec to failure exhibited a corroded grain face and a semicircular pattern, Figure 10. This semicircular pattern was also interpreted as being caused by intermittant crack movement associated with chemical corrosion.

A zone near the tensile surface on a fracture face of a Group I specimen tested in 1M DMF was examined by scanning microscopy techniques. The fracture origin was not located nor were any features located that could differentiate the mechanism of crack nucleation or growth. Figure 11 illustrates one region about 20 um from the tensile surface where the cleavage fracture tracings reveal that the crack front was moving away (in direction of arrow) from the tensile surface. Since this distance is essentially one grain in from the surface, it was concluded that a surface crack caused failure. Furthermore, the crack had probably reached critical dimension and was traveling at high velocity by the time the cleavage fracture tracings were created.

An extensive survey by scanning microscopy was also performed on Group I specimens tested in H_2O and also in DMSO . 10% DMF. No positive identifications of fracture origins were found in either case. This in part spoke for the uniformity of the material and freedom from flaws much larger than the grain size found as fracture origins in many materials. Figure 12 illustrates a zone on a DMSO - 10% DMF fracture surface adjacent to the tensile surface. The saw-toothed cleavage fracture is unusual in polycrystalline materials and may have a similar origin to that observed by Hockey and Groves[18] in single crystal MgO. They attributed this to chemical corrosion at the crack tip forcing the crack front to deviate from a favorable cleavage plane. In the case of a polycrystalline material, the

crack front is influenced by the energy for propagation through adjacent grains as well so it is not clear that the same reasoning can be applied. In fact, several grains near the saw-toothed grain have undergone trans-granular fracture which require shear, a process that probably requires more energy than the saw-toothed higher surface area cleavage fracture. Also note the one intergranular fracture which undoubtedly requires the least energy of the three types illustrated in this one micrograph. The fracture tracings indicate that the direction of crack growth (in direction of arrow) was away from the tensile surface as expected for growth of a surface crack.

IV. DISCUSSION

One concern with the use of machined bend specimen surfaces was the possibility that the surface would be work hardened as discussed by Rice[16] to the point where sub-surface fracture origins would control failure. In this case, fatigue response to the environment would probably not be observed since the environment would not have access to the crack tip. Since pronounced negative slopes were observed particularly on the fatigue curves for Grades II, III, and IV MgO, it was concluded that surface fracture origins were observed. The extremely flat curves for Grade I required more extensive consideration of this question. A sample from each testing environ-ment was examined extensively by scanning electron microscopy. Figures 11 and 12 demonstrate for the cases illustrated that, although the origin of fracture could not be found, the crack front was traveling away from the surface within one grain depth from the surface. Similar observations were noted for the H_2O environment and dynamic test. This, combined with the negative slopes on the fatigue curve, was taken as evidence for surface fracture origins. Rebinder effects of over 30 um would be required to explain the negative slopes of the fatigue curves and sub-surface dislocation

nucleation events resulting indirectly from a work hardened surface layer. Rebinder effects in the order of 10 um have been discussed[17], and more extensive effects seem unlikely.

Figure 4 illustrates marked differences in SCC resistance in H_2O for the four grades of MgO. It would appear that the origin for these differences lie in either microstructural or chemical differences. The specimens were all impermeable since they were $> 99.3\%$ density, and the observed phenomena should not be a consequence of density differences. This view is substantiated by the results of Janowski and Rossi[15] who found evidence for internal attack by H_2O with a corresponding loss of strength for hot pressed MgO having $> 1.5\%$ porosity, but not for specimens $< 0.58\%$ porosity. Further, Grades I and II were the most resistant grades and had the highest porosity. The program did not cover a wide range of grain sizes. Grades I and II were essentially the same grain size and were a factor of 1.6 larger than Grades III and IV. This resulted in their being $\sim 30\%$ less grain boundary area in Grades I and II than III and IV. If corrosion followed grain boundaries, the finer grain size material would possess the greatest slopes. In a qualitative sense, this behavior is followed. However, several factors lead to the conclusion that grain size differences alone do not explain the observed behavior. Firstly, a considerable difference in fatigue behavior was measured between Grades I and II having the same grain size and similarly Grades III and IV exhibit marked fatigue differences with similar grain sizes. A second point is that Grades II and III show somewhat similar fatigue behavior but possess the maximum difference in grain size. Thus, it was concluded that the differences in fatigue behavior in H_2O are not <u>strictly</u> a consequence of grain size differences. The third material property considered to explain the H_2O fatigue curves was chemical composition. Particularly

noteworthy was the very low fatigue slope for Grade I, the purest material followed by Grade II, the next purest grade. The fatigue behavior of Grades III and IV is reversed from the expected behavior based strictly on purity. The electron microscopy of Figure 2 and findings of others[16,31] demonstrate that some impurities segregate at grain boundaries and in fact form discrete second phases. One would expect that the composition of the grain boundary phase would depend on the specific species involved depending on its solid solubility and concentration. Ca^{+2}, Na^{+1}, and Si^{+4}, for example, have extremely low solubilities. It is postulated that stress-corrosion resistance in H_2O is controlled by stress enhanced chemical attack along a grain boundary crack, the material free of a grain boundary phase, or showing very little phase would exhibit the greatest stress-corrosion resistance. If several grades had about the same level of impurity, but basically had a grain boundary phase, slightly different stress-corrosion rates could be observed depending on the rate of stress enhanced chemical attack on the particular grain boundary phase in question. This would explain the apparent reversal in corrosion resistance for Grades III and IV. Weiderhorn and Bolz[32] have shown that different glass compositions have different values of K_{IC}. A dislocation model for crack nucleation would predict that the purest material would exhibit the least lattice resistance to dislocation flow. This effect would predict that Grade I would show the least stress-corrosion resistance rather than the greatest resistance as observed. This, combined with the correlation of behavior with purity and the fractographic evidence for corrosion associated with crack arrest lines, lead to the conclusion that SCC in a H_2O environment is due to a chemical corrosion mechanism with impurity phases in the grain boundaries being the principal point of attack.

Most glass[1,3-6] and crystalline oxide[9-13] materials exhibit static

fatigue limits of $> 0.2 \, \sigma_D < 0.6 \, \sigma_D$; thus, the apparent fatigue limits shown in Figure 4 warrant discussion. MgO Grades III and IV appear to approach fatigue limits in the expected range. The establishment of a fatigue limit cannot be exact because of the scatter and difficulty in collecting data $> 10^6$ sec (11.6 days). However, Grade II and especially Grade I are clearly outside the expected range. One possible explanation is that in high purity MgO, free of grain boundary phases, stress enhanced corrosion builds a layer of coherent corrosion product. This product achieved a semi-stable geometry which extended very slowly under the conditions of these tests. The formation of $Mg(OH)_2$, which is known[33] to have some matching coherent planes with MgO, would seem a likely corrosion product in an H_2O environment. Crack extension may become limited by the rate of OH^- diffusion through this layer. This model would be termed the "passive film" model by terminology common to explaining stress-corrosion in metals.[34] In this model, crack growth rates increase each time the film breaks by any one of several mechanisms, e.g., thermal cycling, mechanical cycling, or lattice strains due to misfit between the reactant and product. The very flat fatigue curve for Group I specimens might be a result of very little breakage of the film. The explanation offered for the less pure grades is that stress corrosion was controlled by corrosion of the grain boundary phase. From the available evidence, this phase may be a silicate glass phase, thus fatigue behavior more in line with that found for glass could be observed. A second model to explain the low slope for Group I specimens is that the mechanism shifted for this group of specimens to an internal dislocation nucleated fracture, for example. It can only be stated that evidence for the latter mechanism was sought by scanning electron microscopy but not found, and the passive film model seems self-consistent and the best explanation at this time.

Testing in DMF and the DMF-10% DMSO was aimed toward further elucidation of the crack growth mechanism, but the question of whether or not the environment could penetrate to the crack tip in the time of the experiment was first addressed. An estimate of the time required for these molecules to diffuse to the crack tip was made by assuming semi-infinite plate diffusion (no radial loss of diffusing species), a $D = 3 \times 10^{-6}$ cm^2/sec which is about the lower limit of self-diffusion of large molecules in liquids[35], a diffusion distance of one grain length (45 μm maximum), and 50% saturation to be effective. These conservative conditions are satisfied in approximately 5 sec, which is a short time compared with the presoak and total time to fracture for all experiments. From a molecular size viewpoint, the longest chain length was calculated to be 5.1 Å and 5.6 Å for DMF and DMSO, respectively. Thus, it appears reasonable from both a size and time consideration that these special environments were present at the tips of surface cracks for these experiments. The negative slopes shown in Figures 5-7, as well as the fracture studies, were taken as evidence for surface initiated crack growth.

The data for Grade I (Figure 6) shows sufficient scatter that it would be difficult to draw firm conclusions. The high σ/σ_D is one of the causes of this scatter, which is related to the distribution of strengths around σ_D. Greater separation in the data for the three environments exists for Grade II material (Figure 7). The approximately three orders of magnitude in time maximum separation in lines appears significant. There is one order of magnitude difference in time between the lines for DMF and DMSO + 10% DMF; thus, with the scatter in strength, the significance of this separation may be questioned. The relative order seems reasonable from a dislocation mobility viewpoint, however. The DMF environment, which should give the least dislocation mobility, gave the shortest times to failure. This would

follow the predicted behavior for the Stroh model where dislocations pile
up at a grain boundary. Under these conditions, greater dislocation mobility
leads to more rapid crack nucleation. Actually any crack nucleation model
requiring the movement of mobile dislocations as an integral part of fracture
would be similarly affected. Examination of the H_2O and 1 M DMF environment
data for Group IV specimens is instructive (Figure 8). The short time high
load behavior indicated that 1 M DMF greatly enhanced the time to failure.
At longer times ($>10^4$ sec), the curves converged and perhaps should be
drawn as one curve with a static fatigue limit of $\sigma/\sigma_D \simeq 0.46$. It may
be noteworthy that the 1M DMF environment also contains OH^- leading to the
possibility of competitive kinetic processes. Is it possible that at high
load, dislocation enhanced crack nucleation proceed, but at lower loads
chemical corrosion by OH^- proceeds at a rate that surpasses dislocation
nucleated fracture? This indeed seems unlikely as Figure 5 shows the various
grades to behave quite differently, and there was no apparent reason for
dislocation processes to behave so differently in comparing Grades II and
IV, for example. The higher purity of Grade II should result in greater
not less dislocation mobility than Grade IV. The finer grain size of Grade
IV does not explain the operation of an inherent MgO dislocation mechanism
at lower relative stresses. Westwood and Latanision[36] found that high
dipole moment complexes also affect the hardness and drilling rate in soda-
lime glass by an absorption induced change in near surface flow behavior.
It was argued in a previous paragraph that the H_2O environment behavior of
Grade IV material was controlled by stress enhanced chemical corrosion of
OH^- at the glass grain boundary phase. Thus it appears reasonable to suggest
that the behavior in 1M DMF is a result of the influence of this environment
on the glass grain boundary phase in a manner analogous to that suggested
by Westwood et al.[36]

-20-

It was concluded that interpretation of the H_2O environment tests based on an extension of a pre-existing crack was valid. The conditions for fracture stress, σ, which must be satisfied as derived by Griffith are

$$\sigma = \left(\frac{2E\gamma}{\pi c}\right)^{1/2} \tag{2}$$

where E is Young's modulus, γ is the surface energy, and C is the flaw size. It is recognized that γ should include a geometrical factor to account for the inclination of the crack path to the stress direction, a term for the energy absorbed by dislocation motion associated with the moving crack (this does not necessarily imply dislocation nucleated fracture), a term for subsidiary cracking, and a term for cleavage step formation. Evans[37] concluded that the dislocation motion term was dominant, accounting for about 9 of the measured 14 J/m^2 in 200 μm grain size MgO.

Using notched bars and slit cracks in 20 μm and 50 μm grain size MgO, Evans and Davidge[29] measured $\gamma \simeq 4$ J/m^2 for 50 μm cracks and increasing to a plateau of $\gamma \simeq 14$ J/m^2 for 400 μm cracks. In the absence of macroscopic flaws, C is thought to be between G/2 and 2G where G is the grain size. Using 2G, the σ_D data of Table II, γ was evaluated by equation (1) with the following results:

Grade	γ, J/m^2
I	10.3
II	16.1
III	7.4
IV	12.5

These values agree reasonably well with those of Evans and Davidge[29] although γ for Grade II is a little large for a 66 μm crack and γ for Grade IV is a little large for a 60 μm crack. This may imply that C was underestimated for these two grades of material.

Since stress intensity factors, K, for polycrystalline MgO have not been determined directly, it may be of some value to report calculated values

based on a Griffith crack where

$$K = \sigma \sqrt{\pi c} \qquad (3)$$

The fast fracture value K_{IC} was calculated from σ_D in Table II. For

consistency and lacking direct measurement of the flaw size, C was assumed

to 2G. The stress controlled cracking (SCC) limit K_{ISCC} was obtained from

a best estimate based on the data of Figures 3 and 4. Stress intensity

versus crack velocity relations were calculated based on these data and are

plotted in Figure 13.

Weiderhorn and Bolz[32] have used directly measured K-V curves to predict

static fatigue curves for several silicate glass compositions. These calcula-

tions agreed qualitatively but not quantitatively with the directly measured

fatigue curves of Mould and Southwick[1]. Thus, it is probably unreasonable

to expect Figure 13 to be more than a qualitative representation of a K-V

curve for the four grades of polycrystalline MgO in a H_2O environment. It

is interesting to note that higher K_{IC} values were calculated for Grades II

and IV than the high purity material, Grade I. However, only Grade II

exceeded Grade I and by a very small margin when it comes to a question of

K_{ISCC}. This, of course, is because of the very low slope to the K-V curve

(or σ/σ_D - t curve) thought to be a result of the high purity and freedom

from a grain boundary phase in Grade I. From a design application viewpoint,

Grade II material is to be preferred over Grade I because of the consistently

higher K. However, from a materials development viewpoint, it would be

advantageous to produce a material with higher σ_D using powder of Grade I

quality. One obvious avenue of approach would be to reduce the grain size

of the product made with this powder.

7. CONCLUSIONS

The rate of stress-corrosion cracking of polycrystalline MgO in H_2O

is strongly influenced by the chemical purity of the body with the highest purity material giving the slowest corrosion rates. SCC in lower purity grades is probably controlled by chemical interaction of OH^- at the crack tip which is thought to lie in a $(CaSiNaAl)O_x$ grain boundary phase, explaining the different corrosion rates for the various grades of material. Static fatigue limits of $0.35 \, \sigma_D$ to $0.5 \, \sigma_D$ are consistent with this conclusion. The highest purity grade tested ($99.98^+\%$ MgO) may not have a discrete grain boundary phase so the low stress-corrosion rates and high static fatigue limit of $\cong 0.83 \, \sigma_D$ may be characteristic of intrinsic SCC in polycrystalline MgO.

When H_2O is present, chemical corrosion is believed to have faster SCC kinetics than possible competing processes. This was demonstrated most clearly for Group II specimens. Testing in DMF and DMSO plus DMF mixtures gave evidence for the operation of the Rebinder effect which is interpreted as resulting from enhanced SCC by a Stroh dislocation model. This condition applies only in the absence of H_2O in the environment and on moderately high purity material ($> 99.92\%$ MgO) where the influence of a discrete grain boundary phase does not dominate. In lower purity material, 1 M DMF may affect the grain boundary phase in a manner analogous to the effect of high alcohols on hardness and drilling rates in silicate glass.

Calculated stress intensity factors qualitatively show that Grade II, a sintered large grain size material, exhibits the best overall behavior in terms of dry strength and static fatigue in a H_2O environment. However, the static fatigue performance and nearly identical K_{ISCC} for Grades I and II suggested that the Grade I, high purity material, would have an advantage if a slightly higher dynamic strength version was produced.

-23-

ACKNOWLEDGMENTS

1. R.E. Mould and R.D. Southwick, "Strength and Static Fatigue of Abraded Glass Under Controlled Ambient Conditions, II", J. Am. Ceram. Soc., 42, 582 (1959).

2. S.M. Wiederhorn, "A Chemical Interpretation of Static Fatigue," J. Am. Ceram. Soc., 55, 81 (1972).

3. J.E. Ritter and C.L. Sherburne, "Dynamic   Static Fatigue of Silicate Glasses," J. Am. Ceram. Soc., 54, 601 (1971).

4. C. Gurney and S. Pearson, "The Effect of the Surrounding Atmosphere on the Delayed Fracture of Glass," Proc. Phys. Soc., 62, 469 (August 1949).

5. J.E. Ritter and J. Manthuruthil, "Static Fatigue of Silicate Glasses," School of Eng., Univ. of Mass. Report No. UM-72-5 (May 1972).

6. W.B. Hillig and R.J. Charles, in HIGH STRENGTH MATERIALS, Ed. V.F. Zackay, John Wiley & Sons, Inc., New York, (1965), p. 682.

7. S.M. Cox, "Glass Strength on Ion Mobility," Phys. Chem. Glasses, 10, 226 (1969).

8. A.G. Metcalfe, M.E. Gulden, and G.K. Schmitz, "Spontaneous Cracking of Glass Filaments," Glass Tech., 12, 15 (1971).

9. L.S. Williams, "Stress-Endurance of Sintered Alumina," Trans. Brit. Ceram. Soc., 55, 287 (1956).

10. S. Pearson, "Delayed Fracture of Sintered Alumina," Proc. Phys. Soc., 69B, 1293 (1956).

11. J.E. Burke, R.H. Doremus, W.B. Hillig, and A.M. Turkalo, "Static Fatigue in Glasses and Alumina," Chapter in CERAMICS IN SEVERE ENVIRONMENTS, 5 ed.. W. Wurth Kriegel and Hayne Palmour III, p. 435.

12. R.J. Charles and P.R. Shaw, "Delayed Failure of Polycrystalline and Single-Crystal Alumina," General Electric Res. Lab Report No. 62-RL-3081M, (July 1962).

13. D.A. Krohn and D.P.H. Hasselman, "Static and Cyclic Fatigue Behavior of a Polycrystalline Alumina," J. Am. Ceram. Soc., 55, 208 (1972).

14. R.J. Charles, "The Strength of Silicate Glasses and Some Crystalline Oxides," in FRACTURE, ed. Averbach et al. John Wiley & Sons, Inc., New York, (1959) p. 225.

15. K.R. Jarowski and R.C. Roel, "Mechanical Degradation of MgO by Water Vapor," J. Am. Ceram. Soc., 51 (8) 455 (August 1, 1968).

16. R.W. Rice, "Strength and Fracture of Hot-Pressed MgO," Proc. Brit. Ceram. Soc., 20, 205 (1972).

17. a. A.R.C. Westwood, D.L. Goldheim, and R.G. Lye, "Rebinder Effects in MgO," Phil. Mag., 16, 505, (1967).

b. A.R.C. Westwood, D.L. Goldheim and R.G. Lye, "Further Observations on Rebinder Effects in MgO," ibid., 17, 951 (1968).

18. D.A. Shockey and G.W. Groves, "Origin of Water-Induced Toughening in MgO Crystals," J. Am. Ceram. Soc., 52, (2), 82 (February 21, 1969).

19. A.E. Gorum, E.R. Parker, and J.A. Pask, "Effect of Surface Conditions on Room Temperature Ductility of Ionic Crystals," J. Am. Ceram. Soc., 41, 161 (1958).

20. R.J. Stokes, T.L. Johnston, C.H. Li, "Effect of Surface Condition on the Initiation of Plastic Flow in Magnesium Oxide," Trans. of Metall. Soc. of AIME, 215, 437 (June 1959).

21. F.J.P. Clarke, R.A.J. Sambell, and H.G. Tattersall, "Cracking at Grain Boundaries Due to Dislocation Pile-up," Phil. Mag., 1, 393 (1962).

22. S.C. Carniglia, " Grain Boundary and Surface Influence on Mechanical Behavior of Refractory Oxides - Experimental and Deductive Evidence," Mater. Sci. Res., 3, 425.

23. T. Vasilos, J.B. Mitchell, and R.M. Spriggs, "Mechanical Properties of Pure, Dense Magnesium Oxide as a Function of Temperature and Grain Size," J. Am. Ceram. Soc., 47, 606 (1964).

24. W.B. Harrison, "Influence of Surface Condition on the Strength of Polycrystalline MgO," J. Am. Ceram. Soc., 47, (11), 574 (November 21, 1964).

25. A.G. Evans and R.W. Davidge, "The Strength and Fracture of Fully Dense Polycrystalline Magnesium Oxide," Phil. Mag., 20, (164), 373 (Aug. 1969).

26. A.N. Stroh, Proc. R. Soc., 223, 404 (1954).

27. C.O. Hulse and J. Pask, "Mechanical Properties of Magnesium Single Crystals in Compression," J. Am. Ceram. Soc., 43, 375 (1960).

28. W.H. Rhodes, D.J. Sellers, R.M. Cannon, and A.H. Heuer, "Microstructure Studies of Polycrystalline Refractory Oxides," Contract N00019-67-C-0336, Summary Report (May 1968).

29. A.R.C. Westwood and D.L. Goldheim, "Mechanism for Environmental Control of Drilling in MgO and CaF$_2$ Monocrystals," J. Am. Ceram. Soc., 51, (3), 142 (March 21, 1970).

30. M.H. Leipold and T.H. Nielsen, "The Mechanical Behavior of Tantalum Carbide and Magnesium Oxide," NASA Report 32-1201 (December 1967).

31. M.H. Leipold and T.H. Nielsen, "Hot-Pressed High-Purity Polycrystalline MgO," Bull. Am. Ceram. Soc., 45, 281 (1966).

32. S.M. Wiederhorn and L.H. Bolz, "Stress-Corrosion and Static Fatigue of Glass," J. Am. Ceram. Soc., 53, 543 (1970).

33. R.S. Gordon and W.D. Kingery, "Thermal Decomposition of Brucite: I,
     Electron and Optical Microscope Studies," J. Am. Ceram. Soc., 49, 654,
     (1966).

34. E.N. Pugh, J.A.S. Green, and A.J. Sedriks, "Current Understanding of
     Stress-Corrosion Phenomena," Martin-Marietta Corp. RIAS Tech. Report 69-3,
     (March 1969).

35. R.C.L. Bosworth, "Transport Processes in Applied Chemistry," John Wiley
     & Sons, Inc., New York, (1956), p. 216.

36. A.R.C. Westwood and R.M. Latanision, "Environment-Sensitive Machining
     Behavior of Nonmetals," Cahpter in THE SCIENCE OF CERAMIC MACHINING
     AND SURFACE FINISHING, NBS Special Publication 348, eds. Schneider &
     Rice (May 1972).

37. A.G. Evans, "Energies for Crack Propagation in Polycrystalline MgO,"
     Phil. Mag., 22, 841 (1970).

86

5661-1   (a)   100X   5722-1   (b)   100X
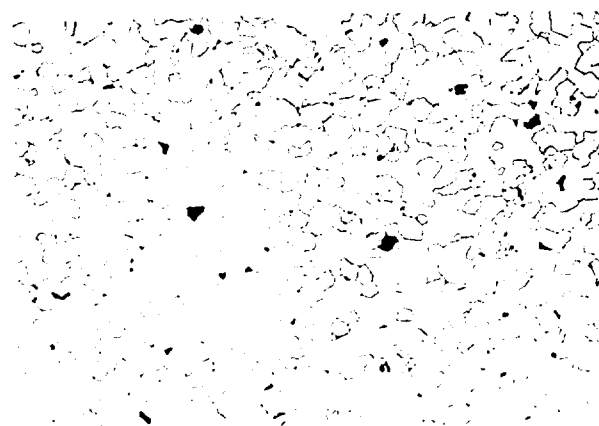
5722-2   (c)   100X   5140-2   (d)   100X

Figure 1. Etched Microstructure of a) Grade I, (b) Grade II, (c) Grade III, and (d) Grade IV MgO.
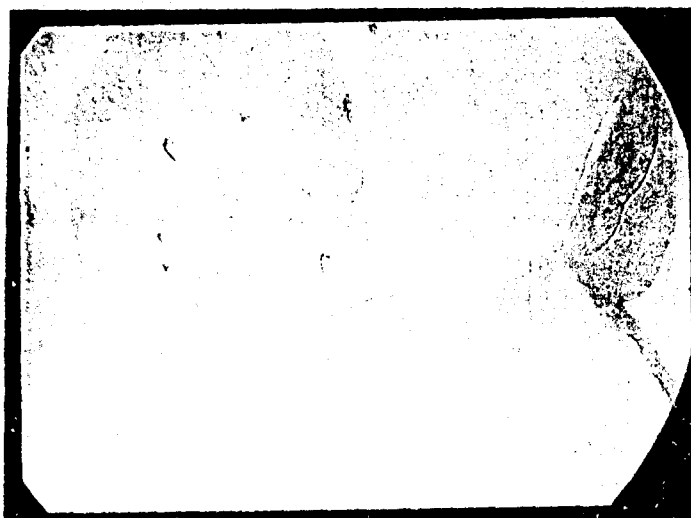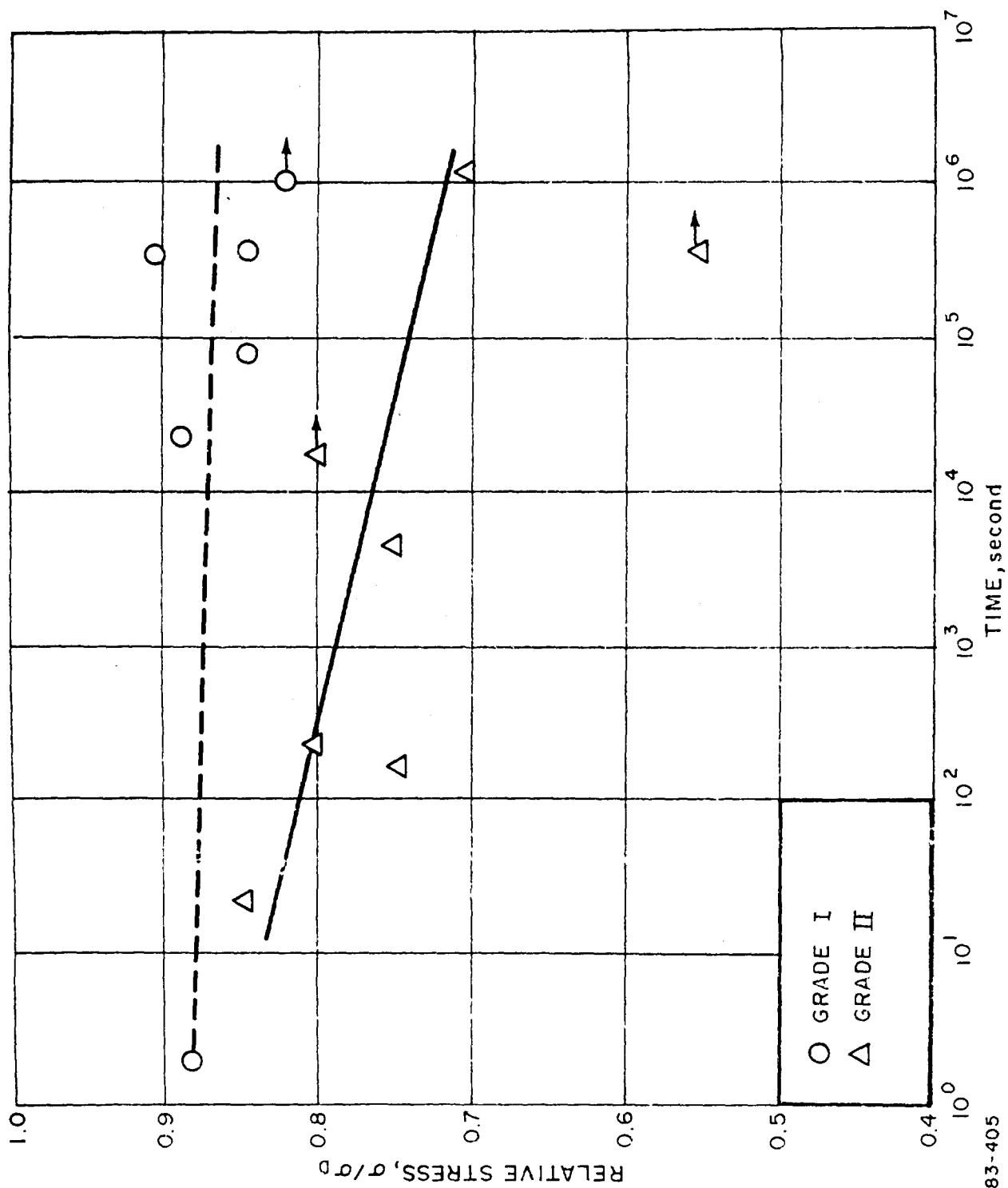
| 72543 | (a) | 7500X | 71048 | (b) | 7500X |
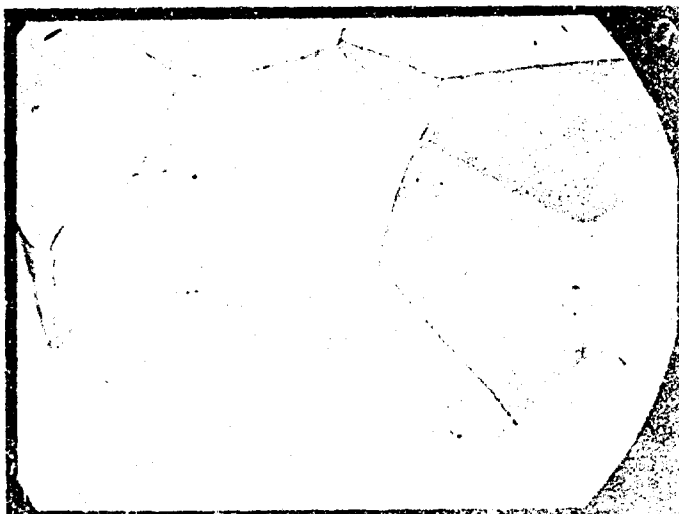
Electron Micrograph of Fracture Surfaces; (a) Grade I,
(b) Grade II, (c) Grade III, and (d) Grade IV MoO.
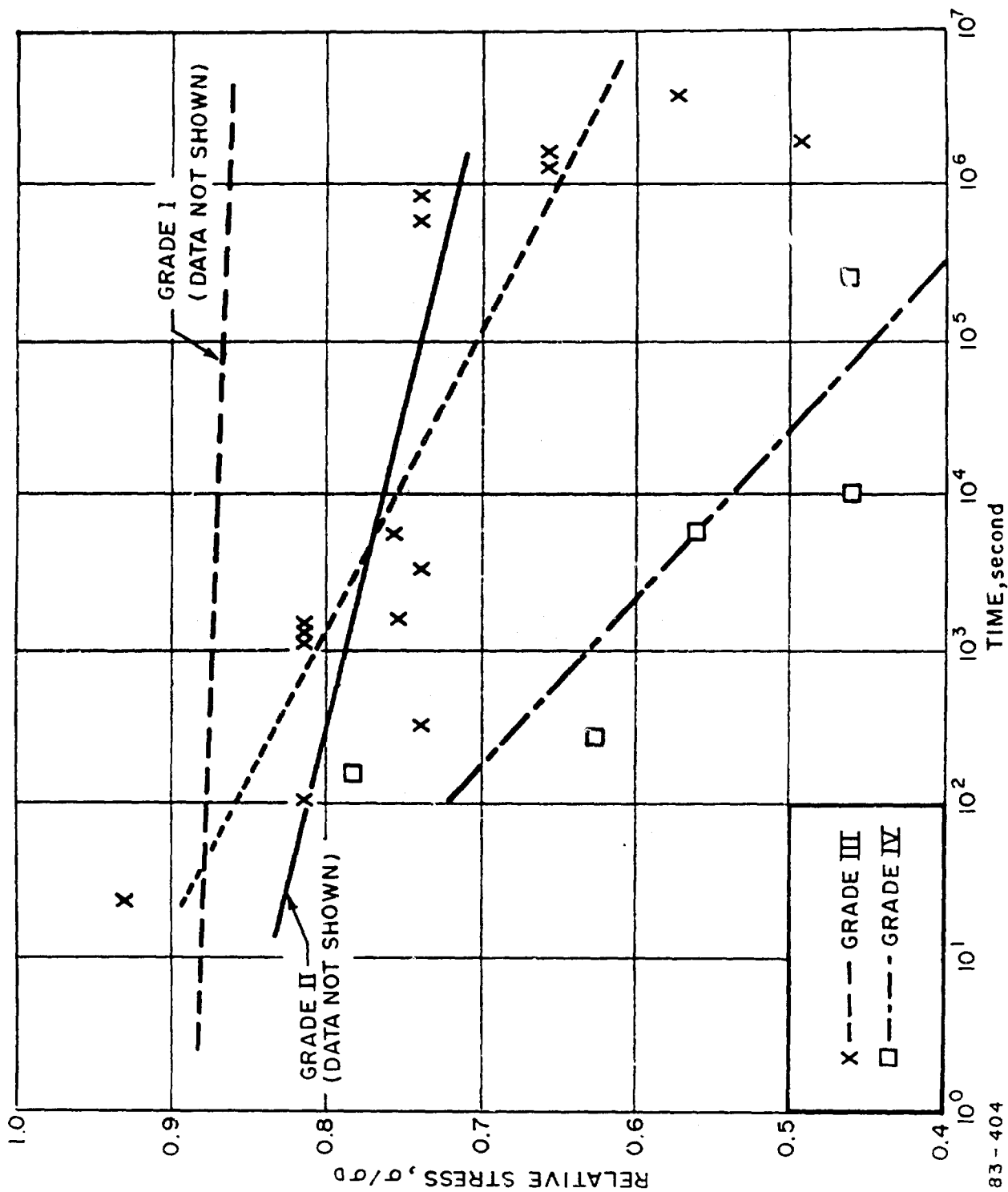
FIGURE 2. DELAYED FAILURE FOR GRADES I AND II MgO in H_2O

GRADE I ○
GRADE II △

TIME, second

RELATIVE STRESS, σ/σ_D

83-405

Figure 4. DELAYED FRACTURE FOR GRADES III AND IV ALONG WITH LINE REPRESENTING GRADES I AND II MgO in H_2O
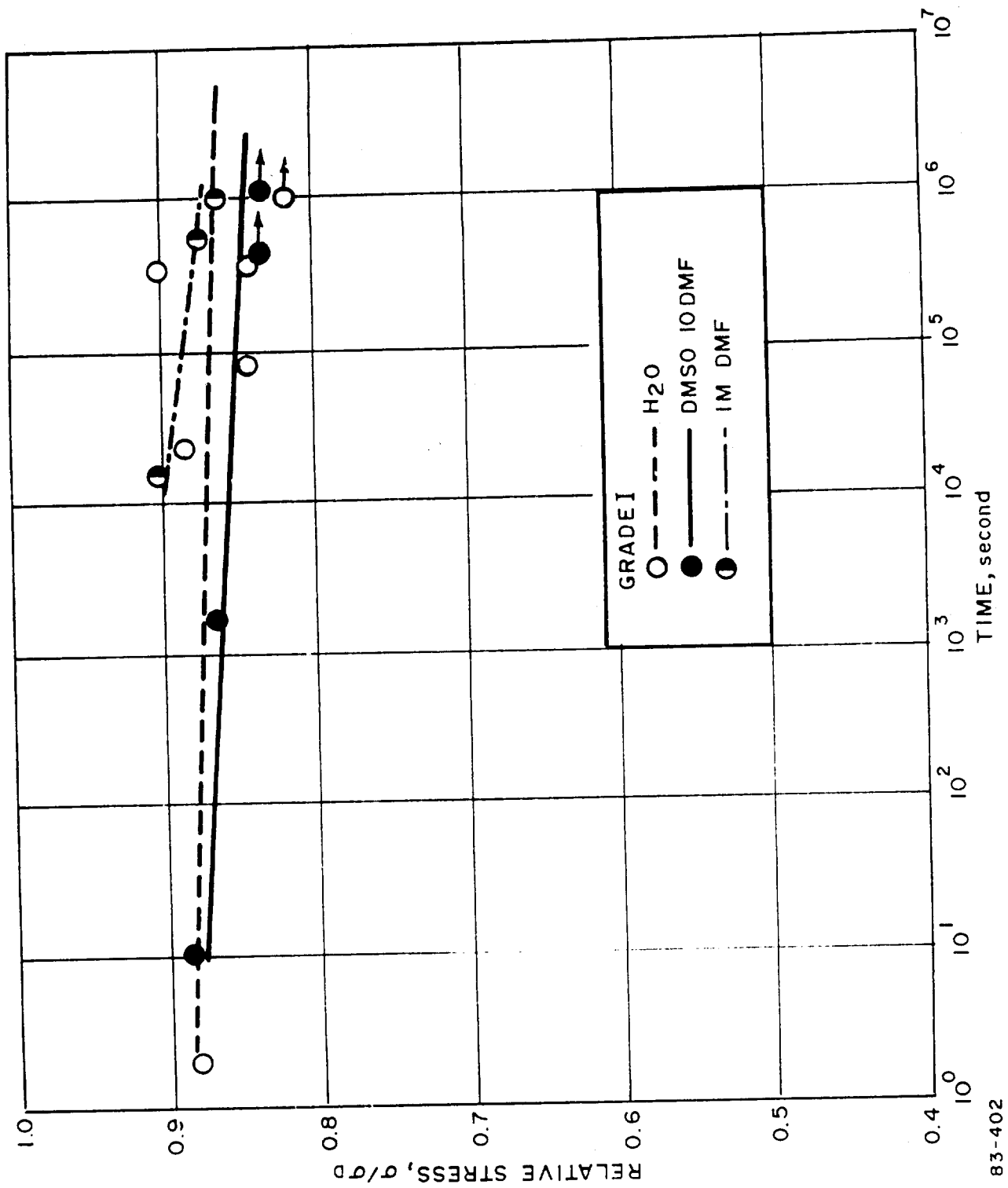
83 - 404
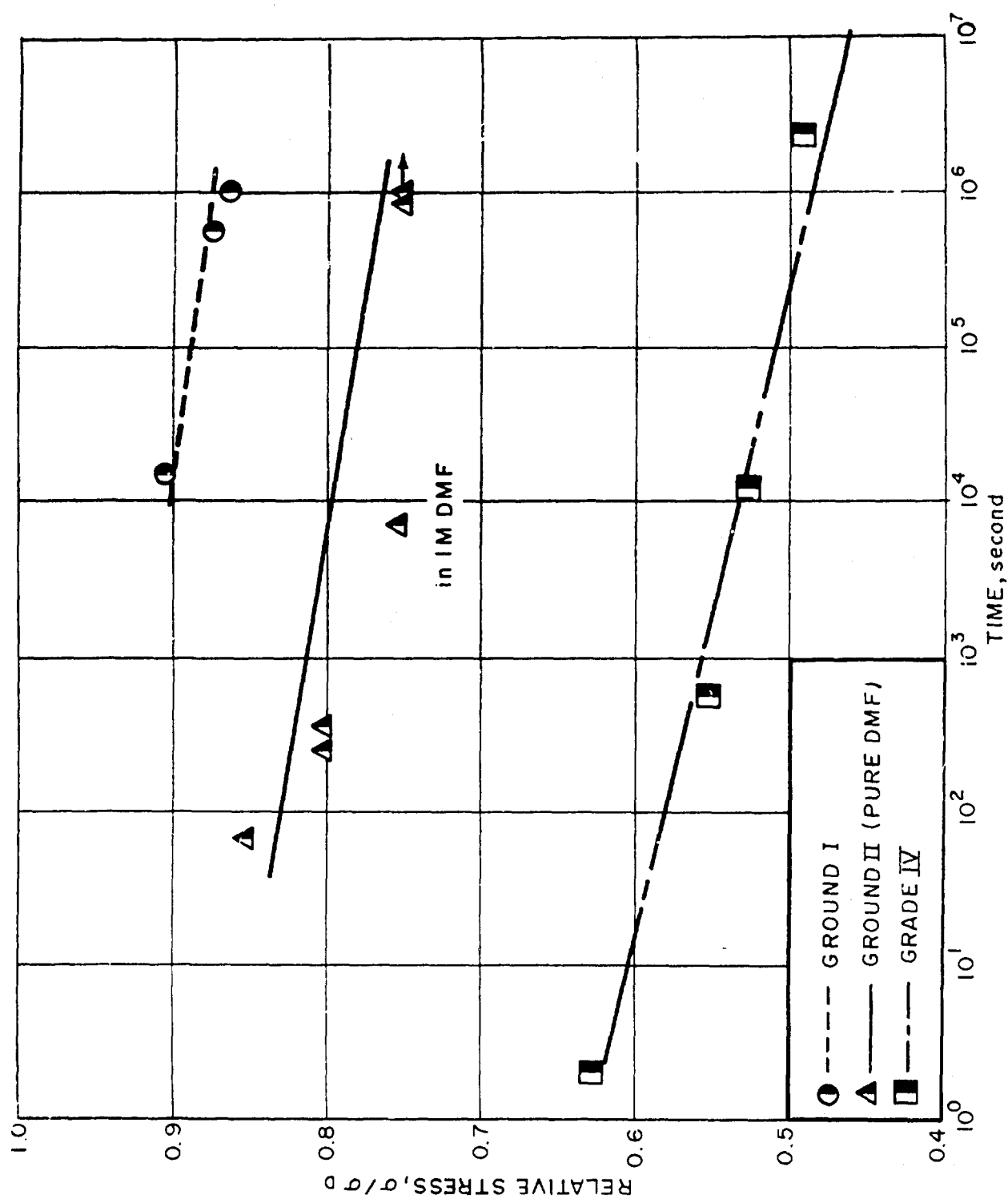
FIGURE 5. DELAYED FAILURE IN 1M DMF.

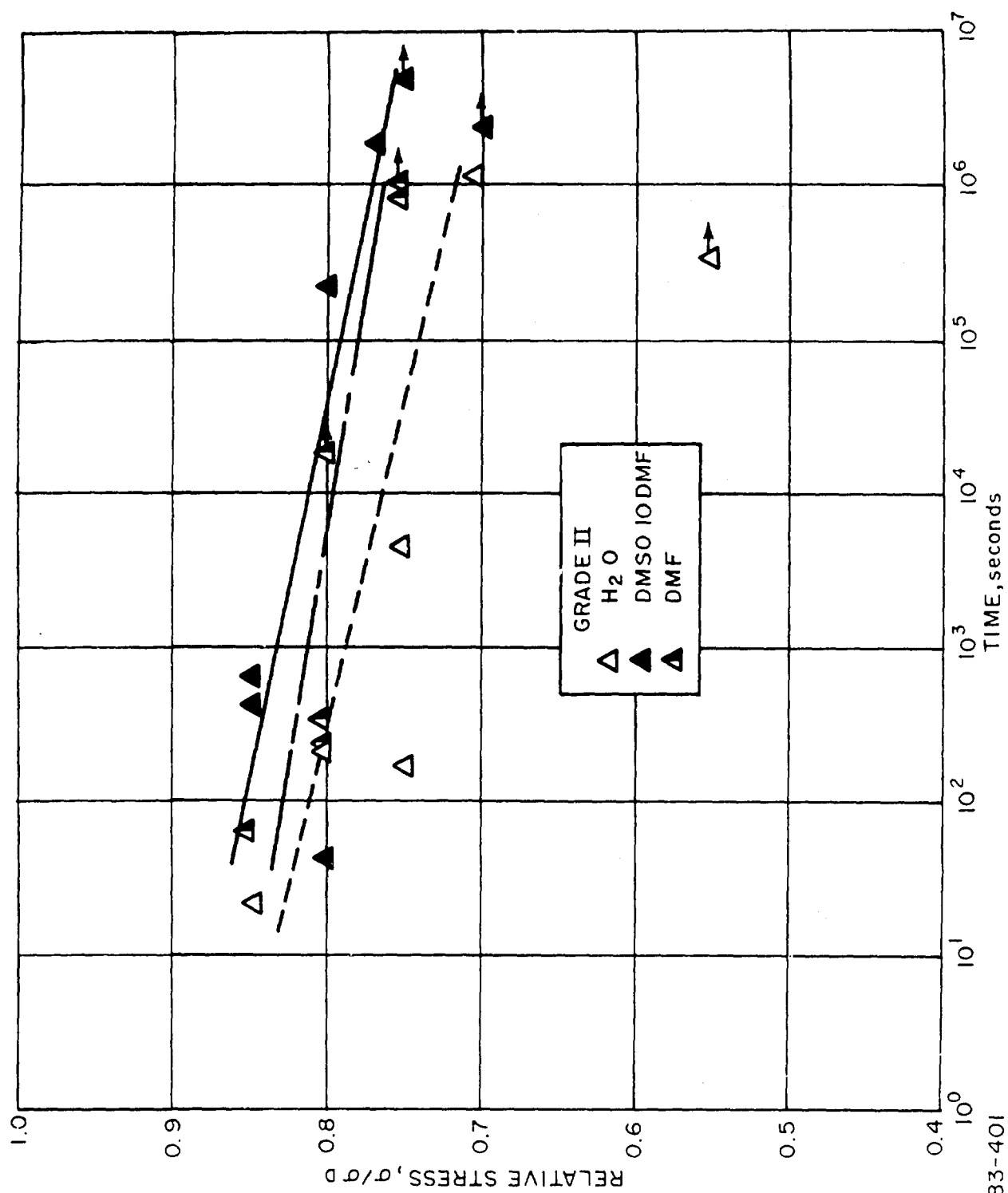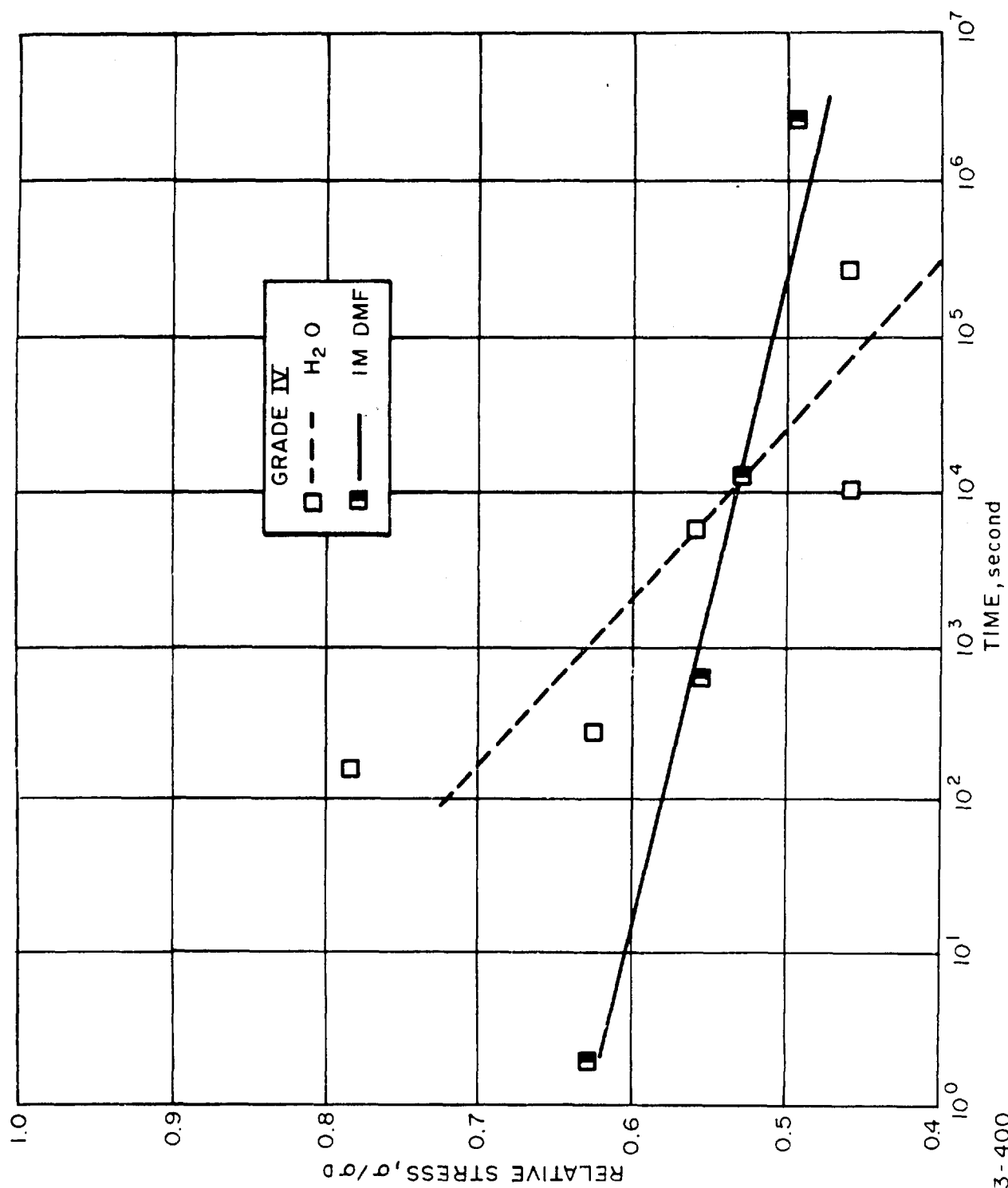FIGURE 6. DELAYED FAILURE OF GRADE I IN H_2O_4, 1M DMF AND DMSO · 10% DMF.

83-402

92

FIGURE 7. DELAYED FAILURE OF GRADE II IN H_2O, DMF and DMSO . 10% DMF.

83-401

FIGURE 8. DELAYED FAILURE OF GRADE IV IN H_2O and 1M DMF.

83-400

71027   (a)   7500X

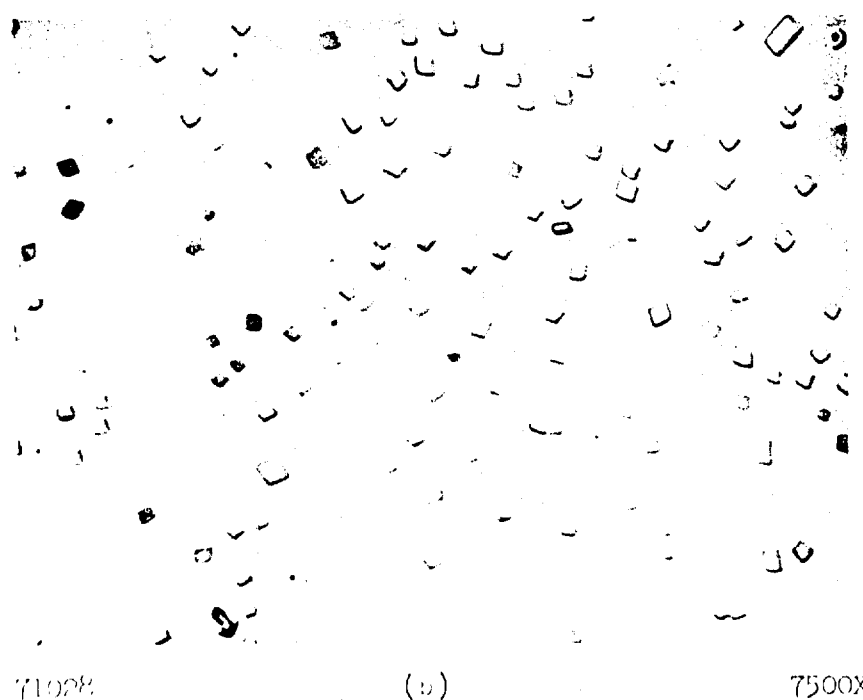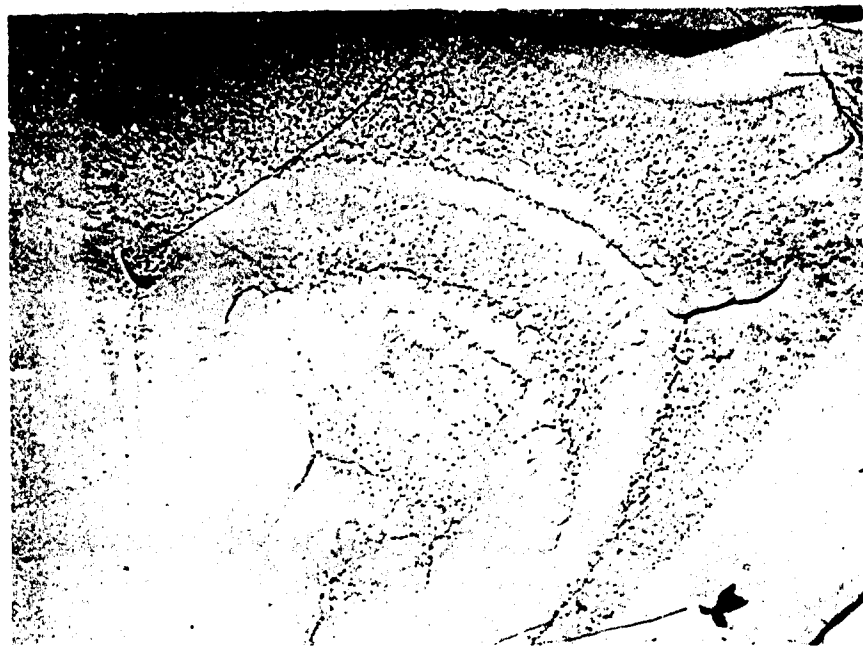71028   (b)   7500X

Figure 9. Fractograph of Group II, 1.2×10^{6} sec H_2O Environment Specimens Exhibiting a) pits associated with crack arrest lines, and b) random flat bottom pits.

691109 7500X

Figure 10. Fractograph of Group II, 6.8×10^3 sec, H_2O
Environment Specimen Corroded Grain Face and
Associated Crack Arrest Pattern.

C-5   1400X

Figure 11. Fractograph of Area Adjacent to Tensile Edge of Group I, [illegible], SCC Environment Specimen showing Direction of Crack Propagation (arrow).

O-2

1900X

Figure 19. Fractograph of a Zone Adjacent to Tensile Edge of Group I, 1.7 x 10⁷ c/s, DMSO-10% DMF Environment Specimen Showing Three Edges of Fracture and Direction of Crack Propagation (arrow).
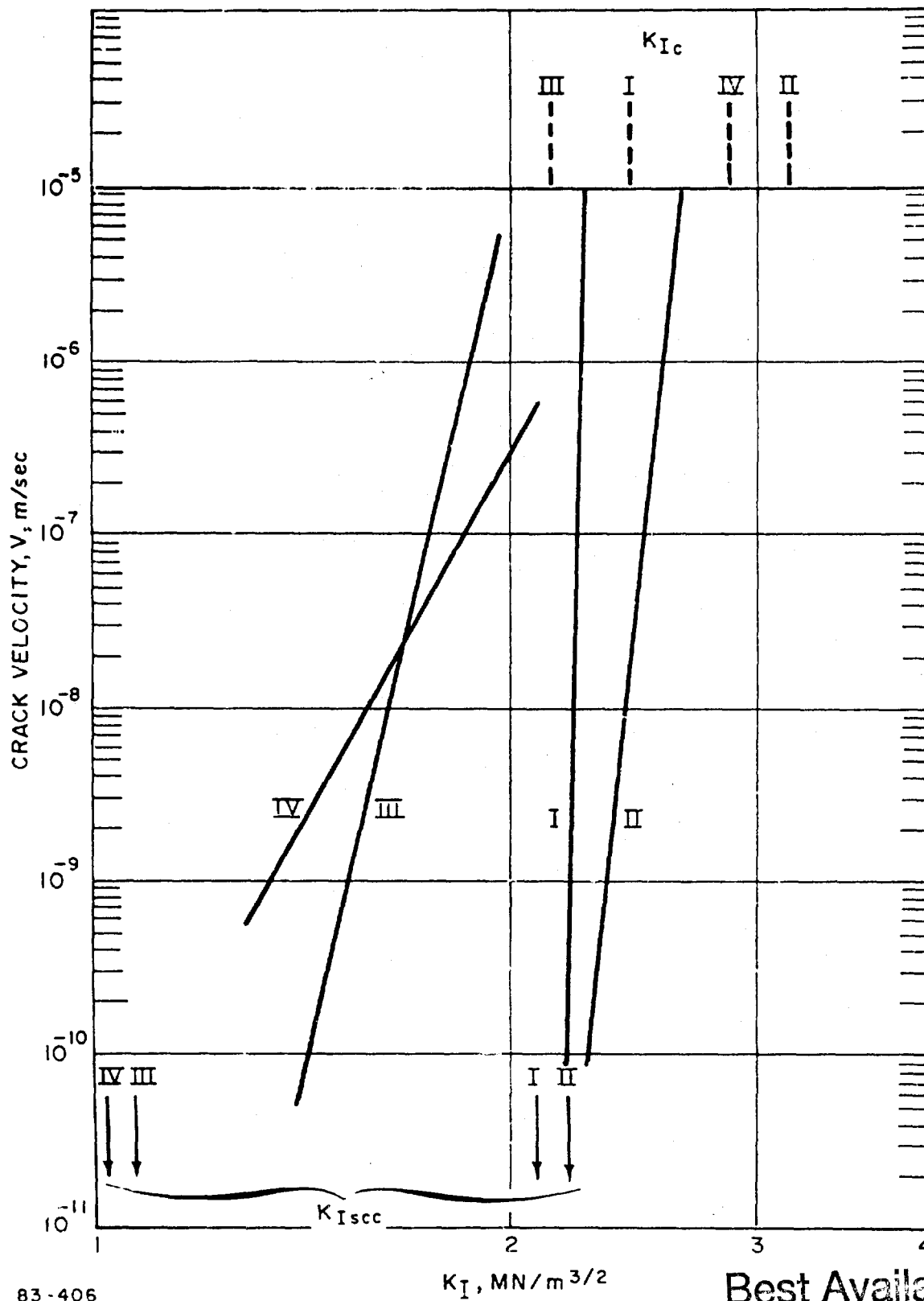
FIGURE 1. STRESS INTENSITY FACTORS CALCULATED FROM FAILURE DATA.

83-406

Best Available Copy